We are IntechOpen, the world's leading publisher of Open Access books Built by scientists, for scientists

4,800
Open access books available

122,000
International authors and editors

135M
Downloads

Our authors are among the

154
Countries delivered to

TOP 1%
most cited scientists

12.2%
Contributors from top 500 universities

CLARIVATE ANALYTICS BOOK CITATION INDEX INDEXED

WEB OF SCIENCE™

Selection of our books indexed in the Book Citation Index in Web of Science™ Core Collection (BKCI)

Interested in publishing with us?
Contact book.department@intechopen.com

Numbers displayed above are based on latest data collected.
For more information visit www.intechopen.com

23

Quality Control and Characterization of Scintillating Crystals for High Energy Physics and Medical Applications

Daniele Rinaldi[1], Michel Lebeau[2],
Nicola Paone[3], Lorenzo Scalise[3] and Paolo Pietroni (formerly with[3])
[1]*Università Politecnica delle Marche/*
Dipartimento di Scienze e Ingegneria della Materia, dell'Ambiente e Urbanistica
[2]*European Organization for Nuclear Research (CERN)/Department PH*
[3]*Università Politecnica delle Marche/*
Dipartimento di Ingegneria Industriale e Scienze Matematiche
[2]*Switzerland*
[1,3]*Italy*

1. Introduction

To the discovery and first use of scintillators are linked the names of W. Crookes, A. Becquerel and E. Rutherford. Since then phosphors have been used to materialise information generated by various scientific, medical and industrial apparata.

Phosphorescence, luminescence and scintillation are basically the same phenomenon, differing by the internal mechanisms involved and by their decreasing time scales. Energy carried by radiative phenomena is converted into light in the phosphor when excited electrons turn back to their equilibrium state by the release of photons in the visible (or near-visible) range. In the first applications, observation was only visual and result qualitative. By their growing demand in space and time resolution, applications themselves prompted the increased performance of the phosphors. The early X-ray radioscopic devices, with their slowly glowing zinc sulphide screens, gave way to faster and safer means of observation.

Thanks to the development of adapted technologies (invention of the photomultiplier tube by Curran and Baker in 1944), light could be converted into electric analog signal and ultimately into manageable data. At that stage, the major interest of the phenomenon i.e. the proportionality of the light output to the incident energy, could be fully exploited. Experimentation in nuclear and particle physics began using plastic and liquid scintillators of increasing light yield and fast response. The discovery of NaI(Tl) in 1949 (Hofstadter, 1949) owed Hofstadter a Nobel Prize. Despite its hygroscopy and radioactive dopant, NaI(Tl) reached mass production scale, and is still in wide use today. With the discovery of BGO ($Bi_4Ge_3O_{12}$) scintillation in 1973, M.Weber and R.Monchamp (Weber, M. & Monchamp, R., 1973) opened the era of fast, dense synthetic mineral crystalline scintillators at the

industrial scale: by 1989 1.4m^3 (11 400 pieces) of BGO had been produced for the L3 experiment at CERN. This achievement initiated the steady supply for a growing medical imaging market. Thanks to focused progress in solid state physics, deeper understanding of the physical phenomenon led to light production levels competing with the best organic scintillators without their weak sides. The role of R&D collaborations and dedicated conference cycles was crucial in this progress (SCINT conferences since 1991, Crystal Clear Collaboration since 1992). Attempts were made to produce amorphous (glass) and even polycrystalline (ceramics) scintillators, to try and gain from available profitable mass production methods. Finally the many advantages of monocrystalline structure has turned to be the mainstream in scintillator development. After NaI(Tl) and CsI(Tl) followed a sequel of new, better performing crystals. BGO, CeF_3, BaF_2, $PbWO_4$, LuAP, LSO, LYSO paved the way of a continued progress in performance but also in quality and quantity, the early formulae mostly thanks to the growing scale of high energy physics instruments, the more recent sustained by the growing demand and important economic prospects of medical imaging equipment.

This new generation of materials is characterised by an excellent time resolution, with a steep rise and short persistence (no afterglow), a chemical structure that guarantees reproducible properties and reliable performance over time and a resistance to working conditions (no aging, radiation resistance). By choosing high Z chemicals, high density crystals can be synthesised, ensuring the tight containment of deposited energy -thus reducing the instrument dimensions. High purity raw materials, sophisticated production processes and adapted quality control methods ensure production of high grade crystals. Among several quality criteria the optical transparency in the scintillation wavelengths is a severe limiting factor as light attenuation and non-uniformity may deteriorate the crystal performance.

Not only intrinsic scintillators have been produced. Passive crystalline lattices have been designed to host specific chemical species –dopants- responsible for the light production, either by themselves or by their specific bonds with the lattice. This is a strong economic incentive as the host lattice may be made of less expensive materials, and budget better spent on costly dopants (e.g. rare earths). The dopant fraction is usually of a few percent. Dopants are selected to match the lattice properties to the best (crystal symmetry, lattice parameters). Two obstacles have to be overcome: segregation that makes light production uneven over the crystal volume, and lattice distortion that may induce mechanical stress and be detrimental to the production yield. Depending on the application and the selected scintillator, crystal sizes may be very different. From bulky 150cm^3 prisms used in high energy physics electromagnetic calorimeters, to mm^3 scale in medical imaging, production problems are quite different and may stress on different features for the optimisation of the material. The latter application has recently seen the development of crystalline fibres of the order of 1mm that may be the present industrial optimum at that scale.

In order to present methods for quality control of scintillating crystals, it is necessary to understand the production process and to identify the characteristic features which determine crystal performance and therefore will be subject to specifications that need to be verified. The following paragraph 2 describes crystal production process, paragraph 3 outlines applications of scintillating crystals, then paragraph 4 treats the methods for quality control based on photoelastic analysis and their applicability to process and product control of crystals. A final paragraph will resume the content of the chapter.

2. Production process of scintillating crystals

Scintillating crystal production has evolved from the chemical laboratory to the industrial plant scale. Crystals are produced by growth methods specific (optimal) of every chemical compound, part size and quantity (Lecoq, P. et al., 2006).

2.1 Raw materials

Upstream the preparation of raw materials is a prerequisite of the ultimate crystal quality. Quality control and traceability have to secure a supply of tightly specified ingredients. Purity is not an absolute criterion but rather an economic compromise of innocuous and poisonous impurities, affecting scintillation (afterglow, light yield) transparency (colour centres) radiation resistance and built-in stress level (cell distortion). Stoichiometric proportions may not be the optimum as some components may be lost during the growth process, either by evaporation in the furnace atmosphere, or by combination with the crucible material.

Raw materials are ground to specific granularity distributions, thoroughly mixed to required proportions. Preparation is completed by melting the components and producing a polycrystalline compound that shall be used to fill the crucible for the growth operation.

2.2 Growth methods

A variety of techniques is used to grow scintillating inorganic crystals. They are all derived from two main methods that shall be briefly described.

2.2.1 Czochralsky method

In Czochralsky method (fig. 1), raw materials are molten in a metallic crucible and kept slightly above fusion point.

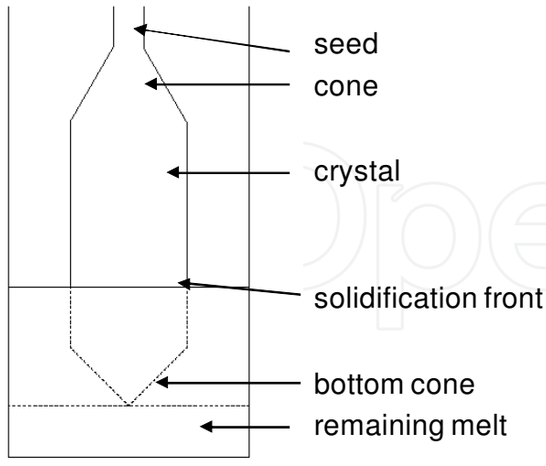

Fig. 1. Czochralsky growth method (pull-from-melt)

A small monocrystal of the same material (seed) is put into contact with the molten bath and pulled up to lift a small meniscus of liquid by capillarity. Solidification occurs at a position and a rate fixed by several parameters. The thermal gradient is regulated by an induction

loop heating the melt with help of the crucible mass. The melt temperature is homogenised by crucible regulation. The growth ("pulling") rate is monitored by a weighting system connected to the seed support. The rising solidified bulk takes the shape of the desired ingot (or boule). The pulling rate gives the ingot its conical top and bottom ends and its cylindrical overall shape. Optimal conditions result in turning the full melt into the ingot volume. The growth of a 1kg PWO ingot took of the order of 1 day. In spite of the circular symmetry of the whole system, the ingot shape may be facetted or oval (fig. 2), depending on the crystal lattice and on the seed orientation. The latter is a critical parameter.

Fig. 2. Czochralsky crystals. The ingot section results from growth parameters and lattice dimensions. Important material scrap is due to difference between ingot and piece, but "peel-like" scraps are recyclable

The crucible is metallic to allow heating by induction. The metal is selected for a high melting point, and for a low chemical affinity with the melt. Platinum is the panacea but poses an economic problem because of its high cost and stock price volatility. The crucible raw material is therefore usually leased from a specialised bank. Even after a large production, the crucible material loss remains small and amounts for a minor fraction of the production cost. Some less expensive metals like palladium or osmium may be used depending on the crystal. The melt free surface is subject to chemical exchanges with the furnace atmosphere, with the risk of losing the design proportions. This is therefore a critical feature of the method and controlled atmosphere is the rule. Depending on the crystal material, vacuum, inert, reducing or oxidizing atmospheres are chosen. For instance, in the case of PWO growth, lack of oxygen induces mechanical stress, whereas its excess is detrimental to crystal transparency.

2.2.2 Bridgman method

This method is an evolution of the fusion zone refining method (fig. 3).
Work piece shape is given by grinding off, powder scrap is not recyclable.
The polycrystalline material is shaped to the final part proportions with extra thickness for the mechanical processing to follow. The shape is usually an elongated prism. A monocrystal seed is placed at one end. This assembly is contained in a thin (a few tenths of a mm) metallic envelope, usually made of platinum. One or several of these assemblies are

positioned in the furnace enclosure. The fusion zone (thermal gradient) moves from the seed interface along the ingot length by combining several induction loops. The gradient displacement velocity is comparable to the Czochralsky growth rate, but the operation has to be repeated several times (at the week scale) to reach monocrystallinity and purity at the required level. The Bridgman process competes with the Czochralsky method only by the use of multiple ingot furnaces. The last passes are considered as an annealing phase. After cooling down the metallic envelope is peeled off and recycled.

Fig. 3. Bridgman crystals. The ingot shape is given by an envelope-like crucible

2.2.3 Annealing

The solidification process results in thermally-induced stresses. They are supposed to have the conventional parabolic profile, with moderate compression in the core, and higher tension at the periphery. The latter is a matter of concern as crystals are especially prone to breaking in tension (crack opening). Annealing is necessary to reduce these tensions. The annealing temperature is very close to the melting point to ease dislocation movements and resolution. The thermal effect is sometimes combined with a chemical one with help of a controlled atmosphere, as a chemical correction is expected to restore the crystal lattice equilibrium. In that case annealing time is governed by diffusion and may take several days. The annealing furnace is therefore a complex device and annealing a costly operation in time and money.

2.3 Mechanical processing

Ingots are the base material for expensive parts tightly specified in shape and dimensions. Mechanical processing is designed to achieve these two goals. For calorimeters, ingots are usually dimensioned for the yield of one piece. Attempts were made to get two and even four pieces out of an ingot. The tiny pixels of medical imaging are either obtained by the many from a single ingot, or cut from fibres.

2.3.1 Cutting (shaping)

The cutting operation provides the part its general shape. Precision is required to limit the amount of material to be removed later by lapping and polishing. It is therefore an economic target to obtain the best geometry (planarity, correct angles) at cutting. Processing

parameters must be optimised to save on time, but not to the price of too thick a damaged sub-surface, and increased risk of edge chipping. The surface finish obtained at cutting ranges from 0,2 to 0,05 μm Ra. Finer finish is not worth doing at cutting as lapping easily produces values below 0,02 μm Ra. A very delicate feature of the cutting operation is the balancing of released thermally-induced tensions as the ingot periphery is removed, face by face. Operations have to be sequenced in such a way that this transitory unbalance is not aggravated (fig. 4).

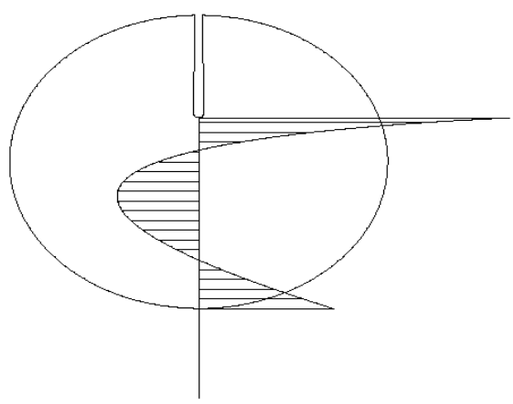

Fig. 4. Effect of cutting on tensional state balance; Cutting a tensioned crystal "frees" mechanical tensions: New boundary conditions transform mechanical tensions into material displacements and deformations, and new mechanical tension distribution. Complex problem with risk of even higher concentrated stresses and breaking when cutting does not follow crystal lattice symmetry

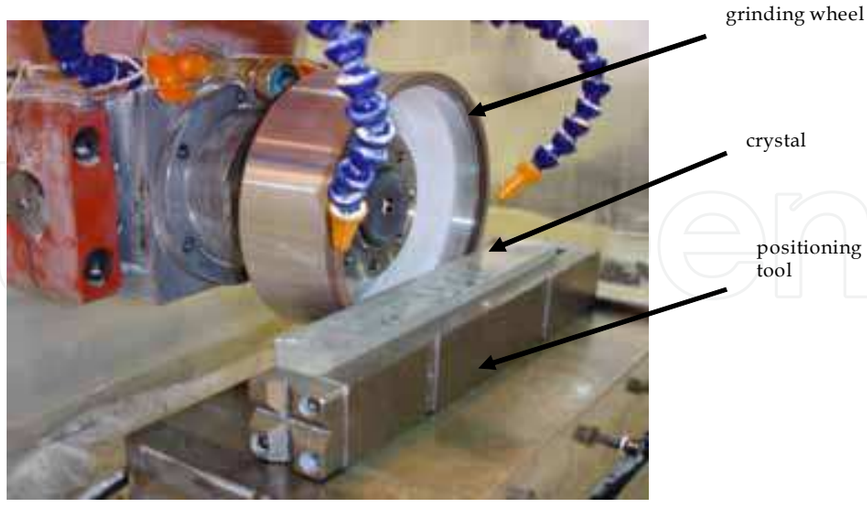

Fig. 5. Crystal shaping by grinding off

Thanks to their transparency, scintillating crystals may be subject to photoelastic stress observation. This method will be discussed in paragraph 4, and it was specifically applied to BGO (Rinaldi et al., 1997) and later to PWO (Cocozzella et al. 2001, Lebeau et al., 2005). The

resulting information, as well as lattice orientation and mechanical properties are critical inputs for determining the processing conditions (Lebeau, 1985, Ishii & Kobayashi, 1996, Pietroni et al., 2005). Grinding-off is the oldest method, that consists in removing excess material by multiple passes of a grinding wheel (fig. 5), on a conventional planar grinder.

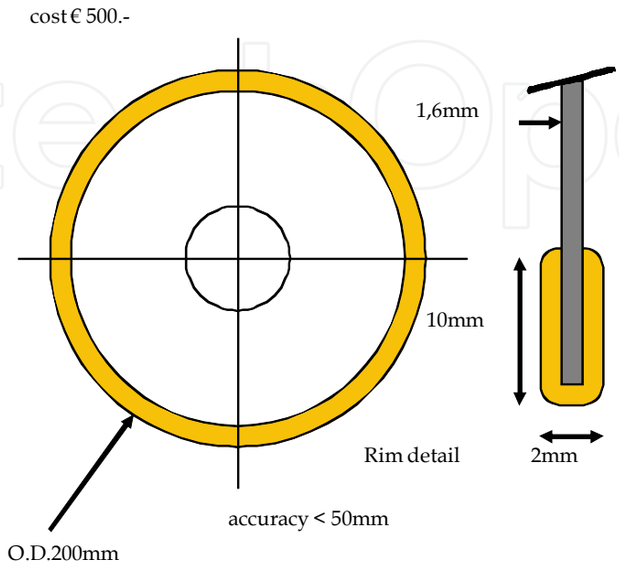

(a)

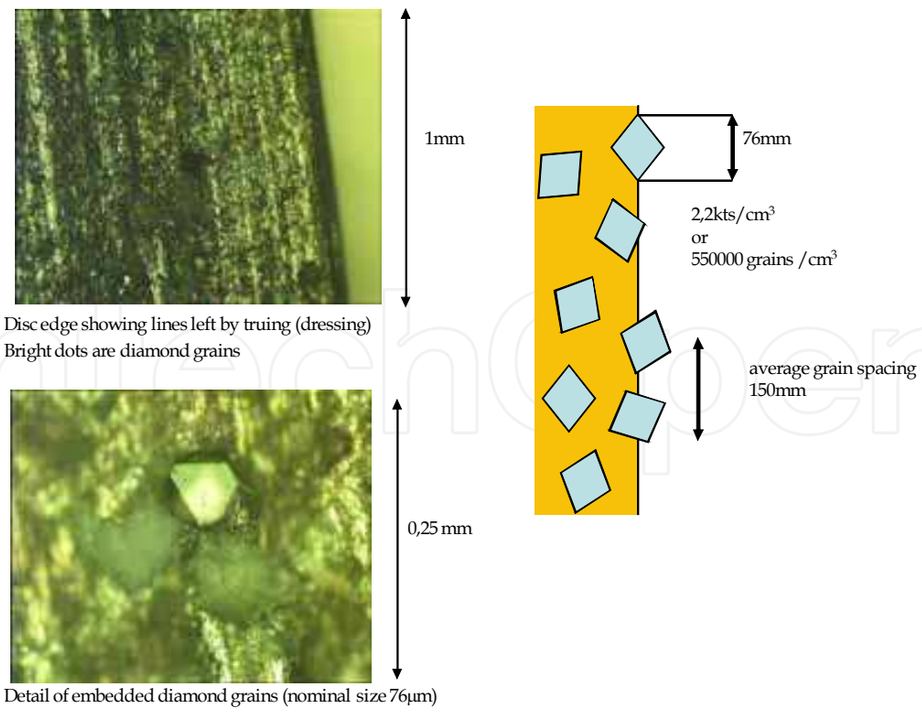

(b)

Fig. 6. Cutting disc (a) and disc details (b)

This is a safe, very accurate but lengthy operation that has been replaced by more economic solutions. Thin disk saws with abrasive-loaded rim are now the most commonplace tool for crystal cutting (fig. 6).
The abrasive grain selection is capital. A good formula is 50 to 100 μm diamond grain sintered in high density in a bronze matrix. The disc diameter is selected to achieve a complete cut in one pass, e.g. 200mm for a 30mm cut depth (fig. 7).

(a)

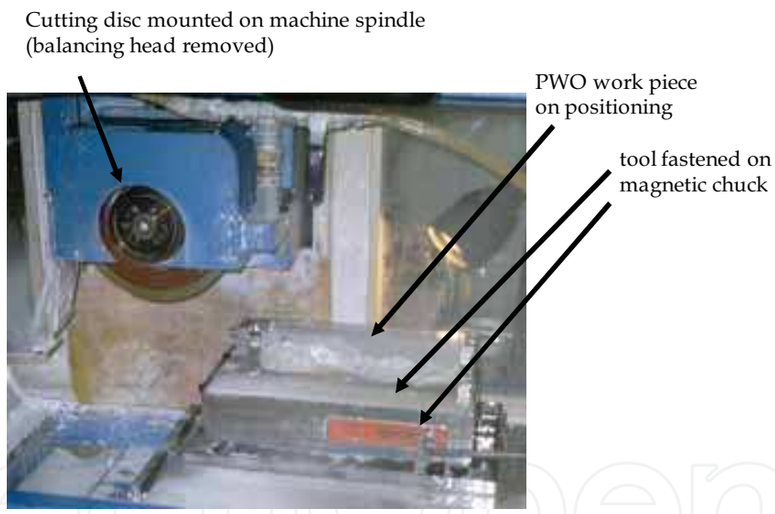

(b)

Fig. 7. Crystal cutting machine (a) adapted grinder, CERN, 2000, detail of cutting machine (b) Details of the cutting machine

The best planarity achieved with this method is of the order of 20 μm, and depending on the tooling and machine quality, a dimensional precision of the order of 50 μm is expected. The disc thickness is a compromise between the cutting precision and the ingot material loss (as fall-off is recycled, but not cutting swarf). The disc thickness also contributes to sub-surface damage depth. A thickness of 2mm is the optimum for a 200mm disc. To achieve the above-mentioned precision the best discs on the market have to be purchased. The machine tool is derived from a conventional grinder, with improved casing for intensive lubrication (fig. 8, a).

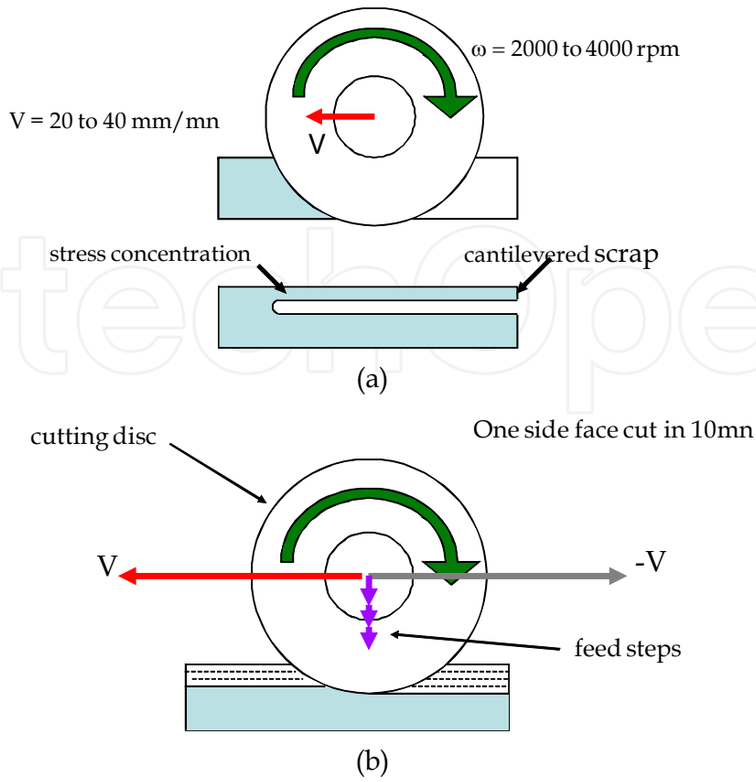

Fig. 8. Full-depth cutting (a); sweeping mode (b) keeps some stress balance

The disc velocity is about 3000rpm, the feed speed about 40mm/min. Sweeping mode: instead of cutting one crystal face in one stroke of the cutting disc, several passes at higher feed (meter per second) with a small vertical take (0,1mm) at every pass are combined for a similar processing time (fig. 8, b). The main advantage is a smaller pressure in the cutting zone, and a balanced release of tensions as the work piece remains symmetrical during the operation. The internal disc saw method was widely used for wafer cutting before the generalisation of plain wire cutting. A very thin (0,3mm) metallic circular membrane tensioned on its periphery is tensioned to achieve a stable planar shape. The edge of the central circular opening is bordered with sintered abrasive grains (fig. 9).

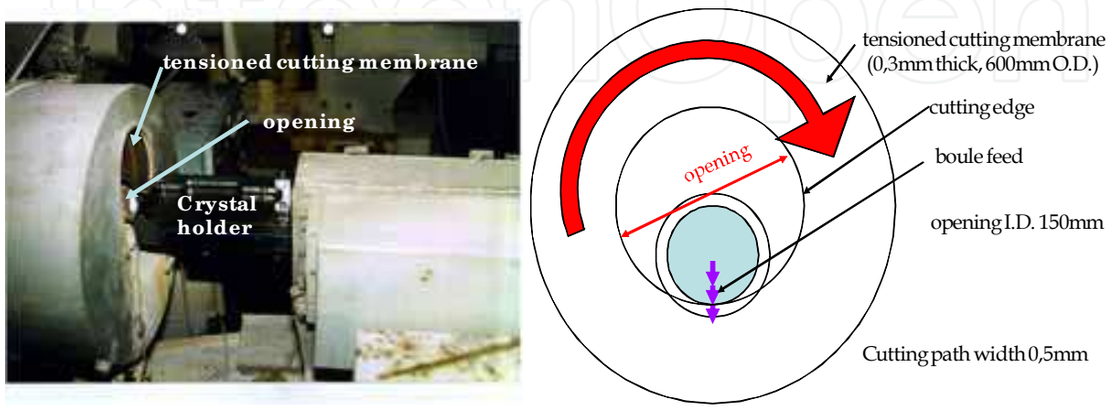

Fig. 9. Inner cutting machine

Only bars of small section compared to the disc opening can be cut with this method. The advantage is an economy in material thanks to the narrow cutting path (disc thickness plus 0,1mm max.). Processing of prismatic pieces is only possible for end cuts. Because of the limited free space within the central opening supporting tooling design is critical.
The plain wire saw method, as said above, is now widely used for mass production of silicon wafers, for electronics as for solar cells. The km long wire runs back and forth and follows a complex path to achieve multiple cutting planes on several ingots (today up to seven with diameters exceeding 320mm). The abrasive slurry (usually cheap corundum) is poured on the wire where it holds by capillarity. The cutting action depends on the grain adherence to the wire, with the result of decreasing efficiency with cut depth. Wire diameter and cutting path are comparable to internal disc saw. This method therefore requires a correction of the planarity afterwards. The specific arrangement of this equipment is only fit for slicing and has no interest for the shaping of prismatic scintillators. Wires with sintered abrasive have been successfully developed to correct the weak sides of the plain wire. Typical diameter is 0,25mm with an 80 µm diamond grain coating. The 2km wire is expensive (1 €/m order) and fragile: processing parameters and lubrication have to be carefully adapted to dedicated machine tools (fig. 10).

Wire length 2km @ 2€/m
Wire O.D. 0,25mm
Diamond grain 80 µm
Wire path 0,3mm
Wire speed 5 to 10m/s
Feed 25 to 50µm/s

Fig. 10. Wire saw (abrasive wire)

Feeds of 50 µm per minute can be achieved with an excellent planarity and a very low sub-surface damage. Parameter optimisation also aims at reducing the wire wear. By combining the feed with the crystal rotation, a symmetric end-cut is possible (cropping), with a balanced stress relief (fig. 11). The machine open configuration allows cutting long side faces (up to 300mm).

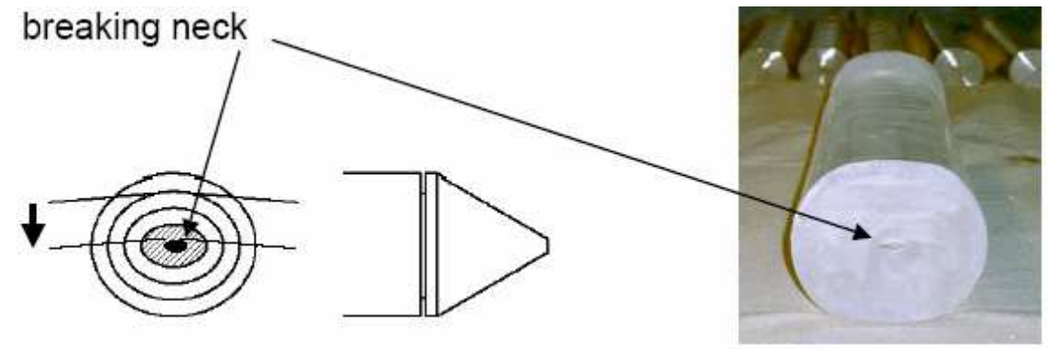

Fig. 11. Rotary wire end-cut (solves boule-ends tensions release); Large ingots have to be put to length before annealing because of annealing furnace dimensions. Cutting un-cured ingots is very delicate and a rotary method is used to keep some symmetry. The cutting wire is slowly fed down while ingot rotates until the end breaks at the thin remaining neck

Crystal cutting is an abrasive process at the microscopic scale. Every abrasive grain works as a gross tool with a negative cutting angle that locally induces high compressive stress. To prevent high crack density and possible propagation, reduce tangential forces, keep work piece temperature low and ease chip removal, the appropriate lubricant must be applied in abundant flow. pH, chemical polarity and affinity may be adapted to the crystal material in a profitable way. Filtering, sedimentation and recycling are environmental constraints.
Lapping is free abrasive action between the crystal face and the surface of a rotary table, the lap (fig. 12).
Combined rotations of the lap and the crystal result in an even distribution of the abrasive action and a regular material removal. Working parameters are the lap and crystal rotation velocities (a few m/s), the pressure exerted on the crystal face (a few N/cm²), the abrasive material and granularity (usually about 15 μm corundum or diamond), the lubricant mixed with the abrasive (slurry) , and finally the lap material. A typical stock removal for PWO was 50 μm/min. With a 0,02 μm Ra finish reached after 3 min, the damaged sub-surface layer from cutting was easily removed. This finish Ra is a good value to start polishing. To prevent edge chipping and resulting deep scratches on the surface, chamfers are necessary on every sharp edge of the crystal before lapping (and polishing): 0,2-0,3mm bevels are usually sufficient. Polishing produces optically transparent faces, that are necessary for scintillating light collection (Auffray et al. 2002). The polish quality can be specified according to a maximum number of visible scratches per view field at a given magnification. The value is far less demanding than for conventional lens polishing. Scintillator polishing operates in similar configuration as lapping. The main differences are the abrasive grain size (from 3 down to fraction of a μm), and the lap cover. Because of the abrasive fine grain, stock removal is slow (less than 1 μm/min) and polishing takes 10 to 20 min per face. This is the critical path in a crystal processing line (Auffra et al. 2002). In mechanical polishing, the material removal results from grain abrasion as for lapping, but at a smaller scale (fig.13). Diamond is the best abrasive in that case. Cooling and lubrication are critical to avoid sub-surface damage.
This method was developed for electronic chips and finds interesting developments for scintillators. The abrasive action is enhanced by specific chemical conditions. For instance, a suspension of very fine grains of quartz (20 nm) in pH9 colloidal silica produces an efficient polishing free of sub-surface damage (Mengucci et al., 2005). Soda and potash were also

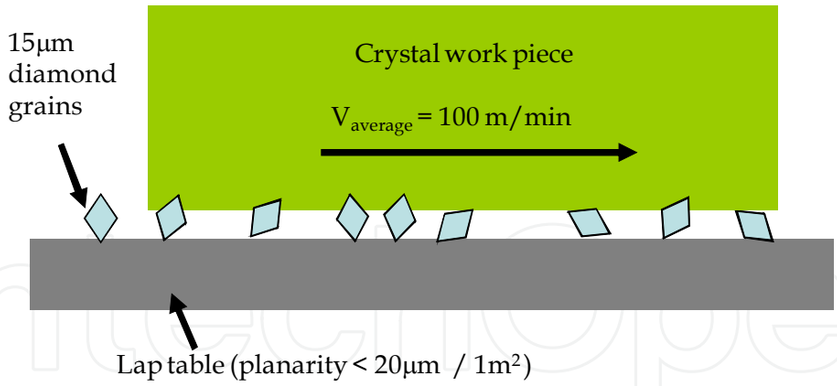

(a)

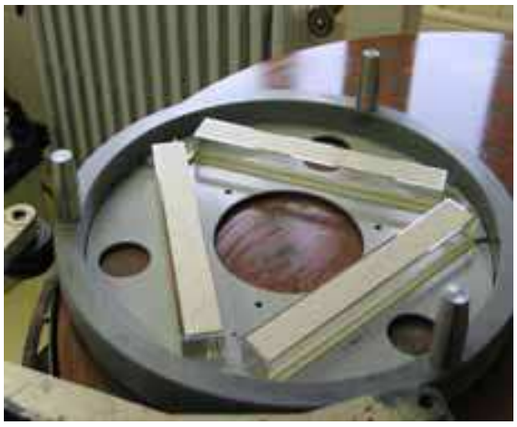

(b)

Fig. 12. Lapping principle (a): Abrasive grains are bumped and tilted between lap and work piece and present fresh cutting edges to work. Lapping tooling (PWO, CERN, 2000) (b): Three crystal shapes are cut out in the lapping mask (or holder). A satellite ring keeps the mask (and crystals inside) in radial position on the lap. Crystal length 230mm, ring I.D. 320mm

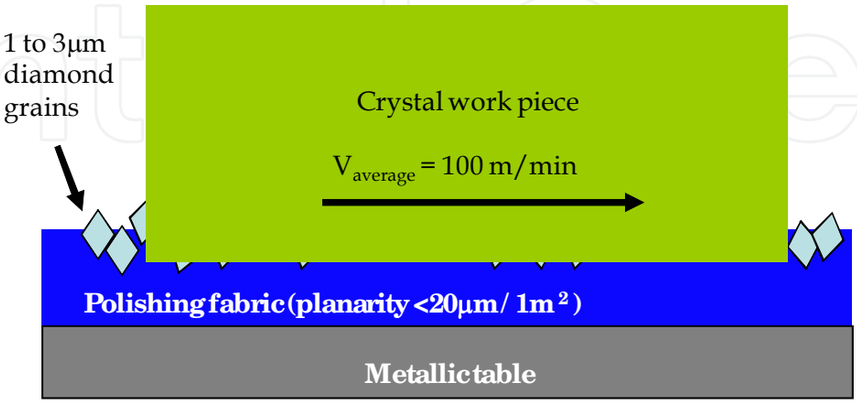

Fig. 13. Polishing schematics. Diamond grains are taken in stable cutting orbits by the fabric. Material removal operates at microscopic scale and some ductile effect results, with limited subsurface damage

tested but surface etching sometimes happened when mechanical action was not properly balanced. The use of aggressive chemicals (bases) poses difficult safety and environment conditions that prevent the spread of these methods. Cerium oxide is known for its combined abrasive action and chemical reaction with conventional lens glass. It is less delicate in use and has been successfully tested with PWO and LSO, but its chemical action remains unclear to date.

3. Scintillating crystals: Applications fields

In recent years, scintillating crystals have found numerous applications in different fields; hereafter we will briefly recall the main areas: Nuclear and high energy physics, medicine (imaging of biological tissues), geology and security.

3.1 Nuclear and high energy physics

This domain is where scintillators were discovered and where most of their development took place. The early 20th century saw their use in fundamental research.

The atomic era opened by the 2nd World War multiplied the use of scintillating counters, also necessary in nuclear energy production. The quick development of fundamental research in high energy and particle physics after the war was a stimulating motivation for increased performance, quantity and economy. The most striking example is in electromagnetic calorimeters (fig. 14), with new projects involving tons of the most recent scintillators (LYSO). Medical imaging benefits of the spin-off of this striving discipline.

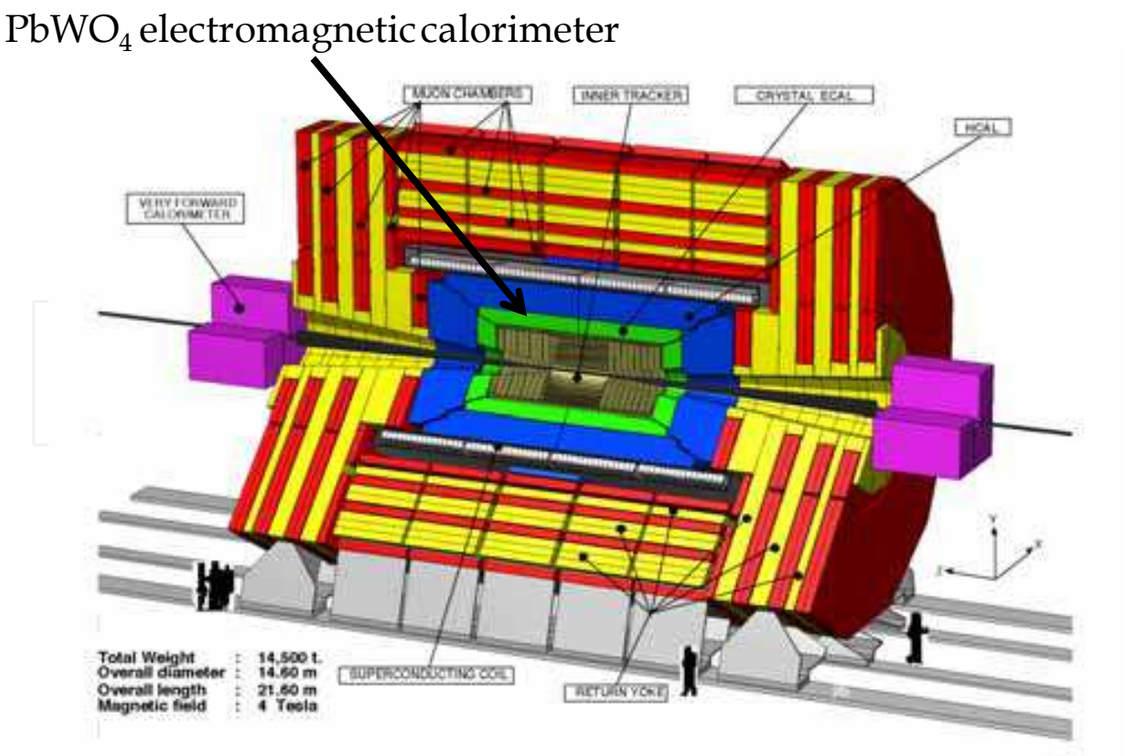

(a)

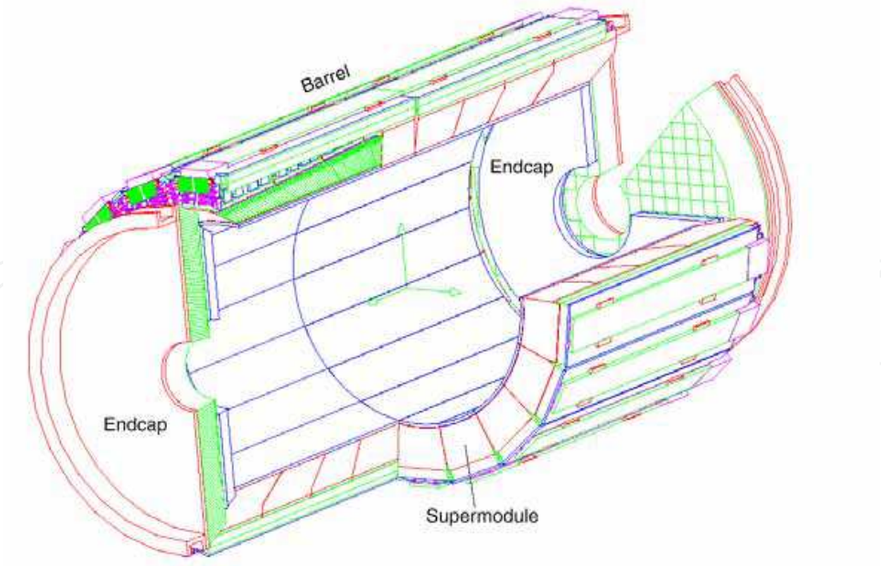

(b)

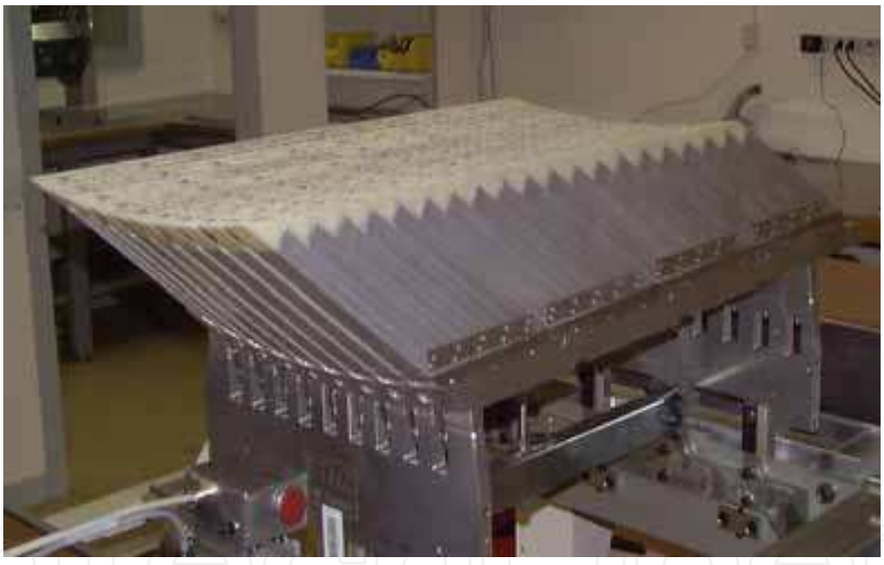

(c)

Fig. 14. The CMS experiment at CERN LHC with $PbWO_4$ electromagnetic calorimeter (a), the CMS $PbWO_4$ electromagnetic calorimeter Modularity crystal sub-module of 10 crystals module of 400 (500) sub-modules super-module of 4 modules barrel of 36 super-modules (b) and (c) a module of the CMS $PbWO_4$ electromagnetic calorimeter (10 x 20 crystals arranged in pointing geometry)

3.2 Medical imaging

Modern radiography is characterised by lower radiation doses (and/or shorter exposures), 3-D information (tomography), real-time observation, tissue or function identification, with the help of large arrays of fine scintillators (pixels) surrounding the patient or covering the organ (mammography) and powerful reconstruction software. The two main types are

projective imaging (e.g. X-ray CT) and PET scanners. In X-ray CT radiation scans the patient from outside and projective information is reconstructed. In PET the patient ingests some radio-element that releases positrons (beta decay). The recombination of the positron with an ambient electron produces two opposite gamma rays of well defined energy detected in opposite scintillator pixels. The radio-element is combined in a chemical (tracer) specific of of tiny 2 x 2 x 10 mm^3 prisms. Processing was dominated by material loss and sub-surface damage because of the crystal scale compared to processing tools. Scintillating fibres are an interesting solution. New fast scintillators with high light output like LuAP, LSO and LYSO are very promising for the medical domain, where economic prospects are high.

3.3 Geologic research

Mining, gas and oil logging are very active economic domains, because of the increasing demand in raw materials and fuel, opposed to the shortage forecast and resulting crisis. Research is performed by prospective drilling. The drill hole may be scanned with two types of detectors. The simpler one is a radiation detector used for the research of radioactive minerals. B.Pontecorvo already proposed such a device with a ionizing chamber counter in 1941. The other type contains a powerful neutron source (Cf, Am, Be, Cs) that irradiates the underground vicinity of the hole. Stimulated gamma emission reaching the detector is typical of the chemical bonds in the mineral (hydrocarbon). Obviously the detector is shielded from the source. The energy spectrum typical of the concerned mineral, and the signal intensity may give a quantitative information. The detector transmits its signal to the recording station on the surface. The source is usually left in the drill hole bottom for safety reasons. Today detectors are of the scintillator type (NaI(Tl), BGO, GSO, LuYAP). Literature is scarce because of patent protection.

3.4 Security

Quick, non-invasive inspection of transport loads, containers, but also luggage and passengers is familiar to everybody in today's life. In the latter case, soft X-ray scanners are used to reveal hidden weapons or hazardous objects, thanks to their density or specific form. Nuclear explosives are also detected by portable radiation detectors. Scintillators are used in these applications. Dual (or multiple) energy systems combined with colour coding display help material identification (different Z) against apparent density. Visual training for qualitative identification are crucial to the efficiency of these detectors. Scientific literature lacks because of patent protection

4. Photoelastic methods for the quality control on scintillating

Paragraph 2 has presented the various phases of crystal production process. It emerges that internal stress distribution is influenced by the mechanical and thermal processes that the crystal undergoes. This brings to the issue of quality control, which implies the assessment of internal stress state in order to set up a proper production process and during its operation.

Residual stress is indeed a major hazard in crystal processing. Crystals are brittle materials, therefore residual tensile stress may easily lead to fracture and breakage during processing or, even worse, during the following assembly of many crystals into complex geometry detectors. Scintillating materials are transparent and usually are optically anisotropic. Internal stress causes lattice strain and deformations, which manifest as stress induced

birefringence; this means that the piezo-optic properties of the material can be observed to verify its internal strain (or stress) state. Photoelasticity is a classical measurement technique suited to observe stress induced birefringence in transparent materials (Wood E., 1964, Dally J. & Riley W. 1987). Therefore photoelasticity is a natural candidate method for quality control of scintillating crystals; of course this measurement method provides only information on quality related to mechanical strain and stress, and requires an accurate knowledge of piezo-optic properties of the material, which is not always available. Furthermore, it is a volumetric technique which provides information on the spatial integral of the stress distribution along the light path through the crystal and not local values.

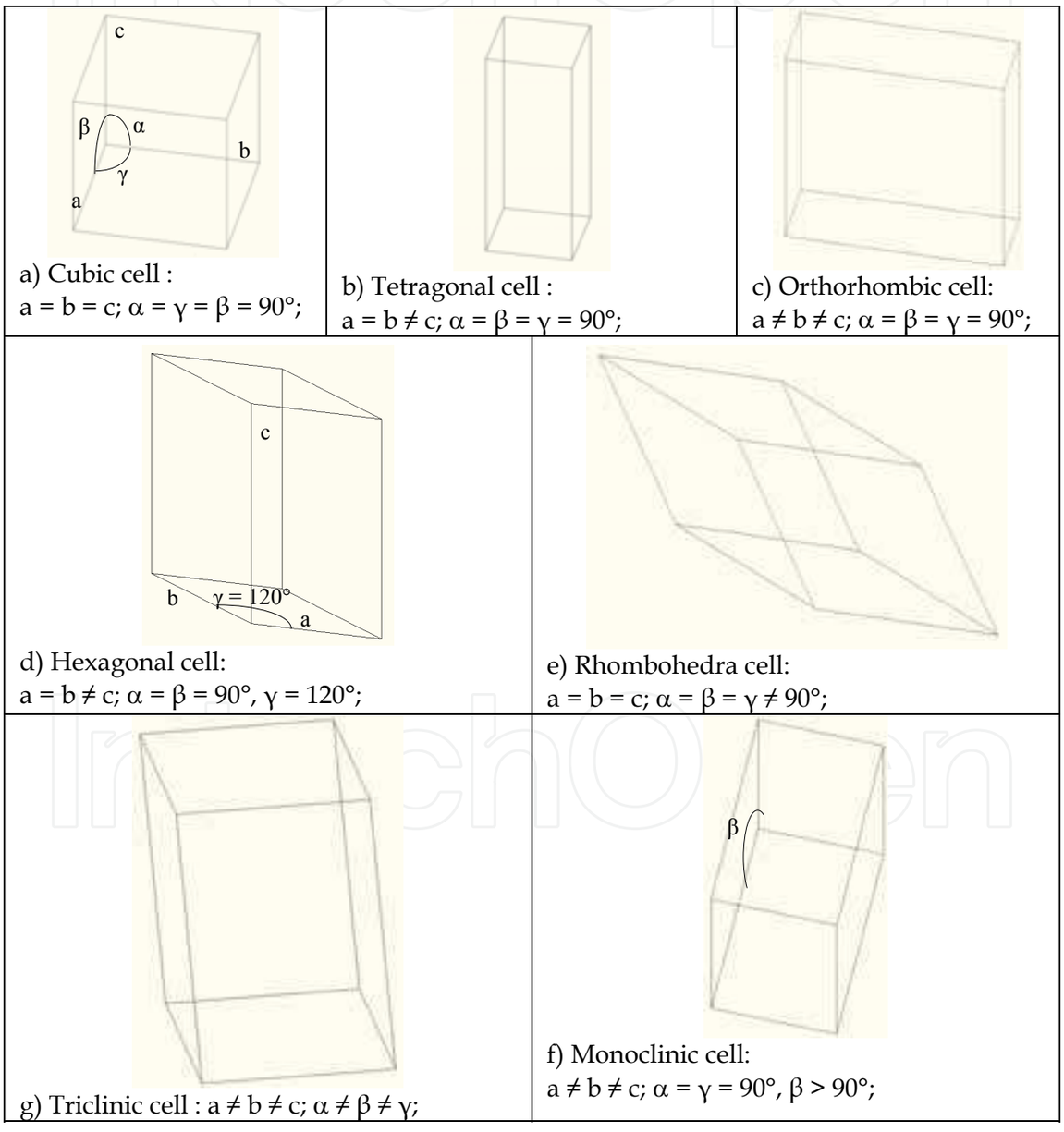

Fig. 15. Geometrical shapes of crystals

Hereafter it is discussed crystal optics, optical anisotropy, piezo-optic behaviour and then photoelasticity is presented for crystal quality control.

4.1 Geometric, mechanical and optical proprieties of crystals

4.1.1 Crystal lattice and symmetry

A crystal is a solid material constituted by a 3D ordered structure which has the name of *crystal lattice.* Each crystal lattice is formed by the repetition of a fundamental element, *the primitive unit cell*: thanks to its replication, it produces the crystal structure (Wood E., 1964, Hodgkinson W., 1997, Wooster W., 1938.). From a geometrical point of view, it is possible to build up the crystal lattice simply translating the unit cell in parallel way with respect to its faces. Indeed the cell geometry should have peculiar characteristics: in particular, the opposite faces should be parallel and, for this reason, it should be a parallelepiped. Possible geometrical shapes are hereafter reported.
The crystal physical and optical properties depend on the typology of unit cell and on the atomic bondages strength. Indeed those properties have the same symmetries of the crystal structure.

4.1.2 Elastic properties of crystals

Crystals undergoing a mechanical stress will deform, so they will exhibit an internal strain distribution. If the mechanical stress is below a limit, named *elastic limit*, crystal deformation is reversible. The strain is proportional with the applied stress for low level stresses. If the crystal undergoes an arbitrary uniform stress $[\sigma_{\kappa\lambda}]$ the generated strain components ε_{ij} is linearly correlated with the stress tensor (Wood E., 1964). This means that:

$$\varepsilon_{ij} = s_{ijkl}\,\sigma_{kl} \quad (i, j, k, l = 1, 2, 3) \tag{1}$$

Equation 1 is the generalized Hook law. Here, s_{ijkl} factors are crystal elastic compliances. The total number of the elastic compliances s_{ijkl} is 81. The Hook law can be written in the following way:

$$\sigma_{ij} = c_{ijkl}\,\varepsilon_{kl} \quad (i, j, h, l = 1, 2, 3) \tag{2}$$

Where c_{ijkl} are crystal elastic stiffness coefficients. The coefficients c_{ijkl} and s_{ijkl} form a forth order tensor. This means that in a coordinate system transformation from a coordinate system X_1, X_2, X_3 to X'_1, X'_2, X'_3 the coefficients s_{ijkl} (c_{ijkl}) are transformed into s'_{mnop} (c'_{mnop}) throughout the law:

$$s'_{mnop} = C_{mi}\,C_{nj}\,C_{ok}\,C_{pl}\,s_{ijkl} \tag{3}$$

where C_{mi}, C_{nj}, C_{ok}, C_{pl} are direction cosine which define the X_1,X_2,X_3 axes orientation with respect to X'_1,X'_2,X'_3. axes. Each s_{ijkl} (c_{ijkl}) coefficient has a precise amplitude and correlation with respect to a specific coordinate system, linked to the crystal. If this coordinate system is coincident with the crystallographic one, the coefficients are the *basic* ones. Since the strain and stress tensors are symmetrical, the tensor coefficients c_{ijkl} and s_{ijkl} are symmetrically coupled according to the subscript *i* and *j*, *k* and *l*, so:

$$s_{ijkl} = s_{jikl}, \quad c_{ijkl} = c_{jikl}, \tag{4}$$

$$s_{ijkl} = s_{jilk}, \quad c_{ijlk} = c_{ijkl}, \tag{5}$$

The equations (4) and (5) reduce the number of independent components of c_{ijkl} and s_{ijkl} to 36. Since c_{ijkl} and s_{ijkl} are symmetrical with respect to the first two subscripts and the second ones, the equations (4) and (5) can be written in more compact way:

$$\left.\begin{array}{l} s_{ij}\ (i,j=1,\ 2,\ 3,\ 4,\ 5,\ 6) \\ c_{ij}\ (i,j=1,\ 2,\ 3,\ 4,\ 5,\ 6) \end{array}\right\} \tag{6}$$

This notation reduces the number of terms of (1) and (2)

$$\left.\begin{array}{l} e_i = s_{ij}s_j\ (i,j=1,\ 2,\ 3,\ 4,\ 5,\ 6) \\ s_i = c_{ij}e_j\ (i,j=1,\ 2,\ 3,\ 4,\ 5,\ 6) \end{array}\right\} \tag{7}$$

but the following rules should be respected:

$$\left.\begin{array}{l} s_{ijkl} = s_{mn} \text{ when m and n are equal to } 1,\ 2,\ \text{or } 3 \\ 2s_{ijkl} = s_{mn} \text{ when m or n are equal to } 4,\ 5,\ \text{or } 6 \\ 4s_{ijkl} = s_{mn} \text{ when m and n are equal to } 4,\ 5,\ \text{or } 6 \end{array}\right\} \tag{8}$$

It is necessary to underline that the symmetry further reduces the number of independent coefficients c_{ij} and s_{ij} . The following formula relates the elastic compliances s_{ij} to the elastic stiffness c_{ij}:

$$s_{ij} = \frac{(-1)^{i+j}\Delta c_{ij}}{\Delta^c} \tag{9}$$

Where Δ^c is a determinant composed of elastic stiffness:

$$\begin{vmatrix} c_{11} & c_{12} & c_{13} & c_{14} & c_{15} & c_{16} \\ c_{12} & c_{22} & c_{23} & c_{24} & c_{25} & c_{26} \\ c_{13} & c_{23} & c_{33} & c_{34} & c_{35} & c_{36} \\ c_{14} & c_{24} & c_{34} & c_{44} & c_{45} & c_{46} \\ c_{15} & c_{25} & c_{35} & c_{45} & c_{55} & c_{56} \\ c_{16} & c_{26} & c_{36} & c_{46} & c_{56} & c_{66} \end{vmatrix}$$

and Δc_{ij} is the minor obtained from this determinant by crossing out the i-th row and j-th column. Likewise:

$$c_{ij} = \frac{(-1)^{i+j}\Delta s_{ij}}{\Delta^s} \tag{10}$$

The following constants are often used for a description of elastic properties of both isotropic and anisotropic media. *Young's modulus E*, characterizing elastic properties of a medium in a specific direction, is defined as the ratio of the mechanical stress in this

direction to the strain it produces in the same direction. The *Poisson ratio* ν is defined as the ratio of the transverse compression strain to the longitudinal tensile strain caused by a mechanical stress. The *Shear modulus* μ is defined as the ratio of shear stress and shear strain, it produces in a material. In isotropic bodies only two of the above-mentioned constants are independent. For this reason, elastic properties of isotropic bodies are often described using the constants λ and μ, called the *Lame constants.* The constant λ and μ are related to the stiffness matrix components as follows:

$$\mu = \frac{c_{11} - c_{12}}{2} \tag{11}$$

$$\lambda = c_{12} \tag{12}$$

Considering the matrix (s_{ij}) then it is possible to write the following formulas E and μ in isotropic case:

$$s_{11}=1/E, \quad s_{12}= -\nu/E \tag{13}$$

$$2(s_{11}- s_{12}) =1/\mu \tag{14}$$

In anisotropic medium Young's modulus in a arbitrary direction X'_3 is:

$$E = 1/s'_{3333} \tag{15}$$

where $s'_{3333} = C_{3i}\, C_{3j}\, C_{3k}\, C_{3l}\, s_{ijkl}$ and C_{3i} ,C_{3j} ,C_{3k} ,C_{3l} are the direction cosine of the axis X'_3 with respect to the crystallographic coordinate system and s_{ijkl} are the basic compliances referred to crystallo-physical coordinate system. Young's modulus is a function of direction for all crystallographic classes, including cubic class.
In anisotropic media the Poisson ratio is equal to

$$\nu^{hk} = \frac{s_{hk}}{s_{kk}} \tag{16}$$

and it represents an estimation of lateral compression parallel to X_h with respect to accompanied elongation parallel to X_h .

4.1.3 Piezo-optical properties of crystals

The piezoptical effect consists of changes in the optical properties of crystals throughout static and alternating external mechanical stresses and it is described in terms of the index ellipsoid. The general equation of the index ellipsoid in an arbitrary coordinate system X1, X2, X3, whose origin coincides with that of the main (crystallophysical) coordinate system, can be written in the following form:

$$B_{11}x_1^2 + B_{22}x_2^2 + B_{33}x_3^2 + 2B_{23}x_2x_3 + 2B_{13}x_1x_3 + 2B_{12}x_1x_2 = 1 \tag{17}$$

Where B_{ij} are the dielectric impermeabilities or polarization constants. Equation 17 is related to anisotropic crystal without any applied mechanical stress.

An applied mechanical stress produces variation ΔB_{ij} in the dielectric impermeabilities:

$$\Delta B_{ij} = B_{ij} - B_{ij}^{0} \tag{18}$$

Considering a first-order approximation, the increments in the dielectric impermeability tensor components are proportional to mechanical stresses:

$$\Delta B_{ij} = \pi_{ijkl}\sigma_{kl} \tag{19}$$

On the other hand, the same increments can be expressed in terms of strain:

$$\Delta B_{ij} = p_{ijkl}\varepsilon_{kl} \tag{20}$$

Such a change in the optical index ellipsoid of the crystal due to the straining is called the elasto-optical effect. The coefficients π_{ijkl} and p_{ijkl} form a rank four tensor and they are called the piezo-optical and elasto-optical constants, respectively. In the matrix notation eqs. (19) and (20) can be rewritten in the following form

$$\Delta B_{m} = \pi_{mn}\sigma_{n} \tag{21}$$

$$\Delta B_{m} = P_{mn}\varepsilon_{n} \tag{22}$$

where if n = 1, 2, or 3:

$$\pi_{\mathrm{mn}} = \pi_{\mathrm{ijkl}}$$

while if n= 4, 5, or 6:

$$\pi_{\mathrm{mn}} = 2 \cdot \pi_{\mathrm{ijkl}}$$

and P_{mn} are the elasto-optical coefficients, $P_{mn} = p_{ijkl}$ for all m and n. In the general case:

$$\pi_{\mathrm{mn}} \neq \pi_{\mathrm{nm}} \quad P_{mn} \neq P_{nm}$$

The piezo-optic and elasto-optic coefficients are related by the following formulas:

$$\mathrm{P}_{\mathrm{mn}} = \pi_{\mathrm{mr}}\mathrm{c}_{\mathrm{rn}}, \quad \pi_{\mathrm{mn}} = \mathrm{P}_{\mathrm{mr}}\mathrm{s}_{\mathrm{rn}}$$

Where c_{rn} are the elastic stiffness and s_{rn} are the elastic compliances.

4.1.4 Isotropy and anisotropy in crystal optical properties

As it is described in previous paragraphs, the symmetry on the crystal lattice influences the symmetry on the optical properties. The Isotropy and anisotropy affect changes on refraction index and the consequent variations of the light velocity with respect to the direction inside the crystal material. Crystals, having a cubic cell, can be considered isotropic for their optical properties. All the rest of crystals cells has an anisotropic behaviour in terms of optical properties (Wood, E. 1964, Hodgkinson I., 1997, Wooster W., 1938). The optical anisotropy allows to classify crystals in two categories: uni-axial anisotropic crystals and biaxial ones

according to the index ellipsoid which provides the value of the refraction index along a specified direction in the crystal (Wood, E. 1964, Hodgkinson I., 1997).
A fundamental representation of *Uniaxial anisotropic crystals* is the *optical indicatrix* or *ellipsoid of the refraction indices*. As far as the uniaxial crystal, there are two principal indices: *ordinary index of refraction n_o and extraordinary index of refraction n_e*. Indeed the optical indicatrix is a rotation ellipsoid, where the both the axes are proportional to n_o *and* n_e. It is possible to state that an indicatrix is positive, when $n_e > n_o$, and negative, when $n_e < n_o$.

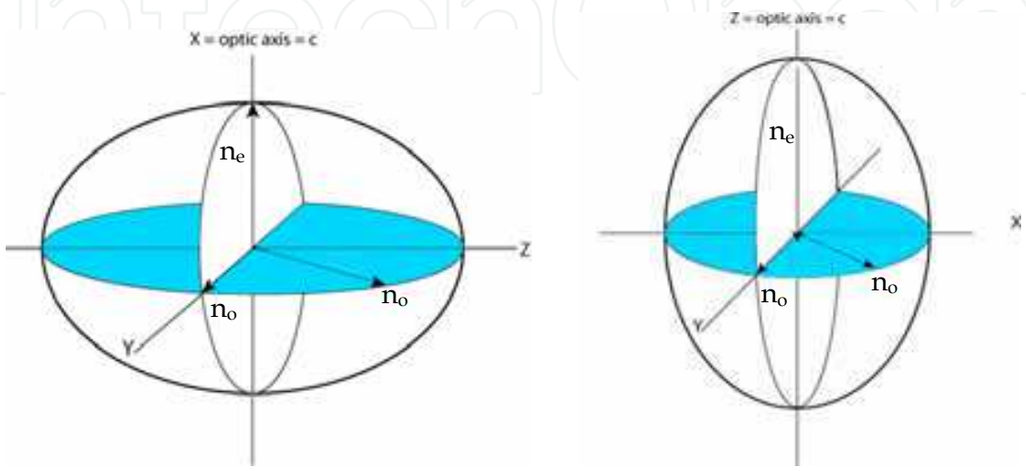

Fig. 16. Optical indicatrix for uniaxial positive and negative crystal

Hereafter three examples (fig. 17-19) are reported in order to explain the concept of uni-axial anisotropy and consequently of birefringence, assuming to study a positive crystal. In first case (fig. 17), the crystal lattice is oriented so that the optic axis is along the light travelling direction. In this case, considering the indicatrix its section perpendicular to the wave vector is circular with radius is n_o. Since in all the vibration direction of the electromagnetic field the refraction index is constant the birefringence is zero.

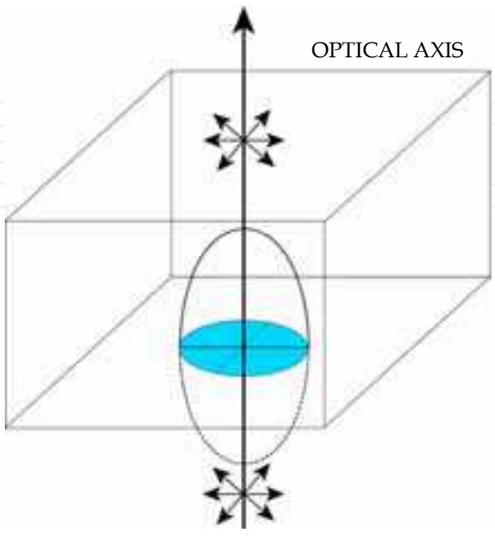

Fig. 17. Uniaxial crystal first example

In the second example (fig. 18), the crystal lattice is oriented in a random orientation so that the light path is at angle θ to the optic axis. The section through the indicatrix parallel to the incoming light wave is an ellipse whose axes are n_o and n_e. The extraordinary ray electromagnetic field vibrates parallel to the trace of the optic axis as seen from Fig. 18, while the ordinary ray one vibrates at right angles.

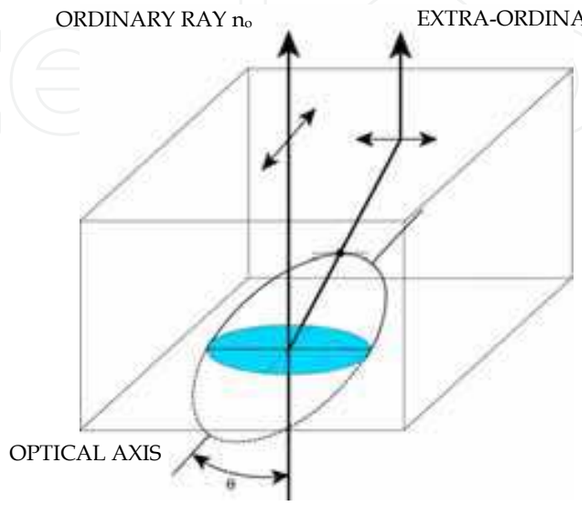

Fig. 18. Uniaxial crystal second example

In a third case (fig. 19), the crystal lattice is oriented so that its optic axis is parallel to the light wavefront. Because the optic axis has this orientation, this section is a principal elliptic section whose axes are n_o and n_e. The ordinary ray therefore has index of refraction n_o and the extraordinary ray n_e, which is its maximum because the crystal is optically positive. The extraordinary ray vibrates parallel to the trace of the optic axis (c axis) and the ordinary ray vibrates at right angles.

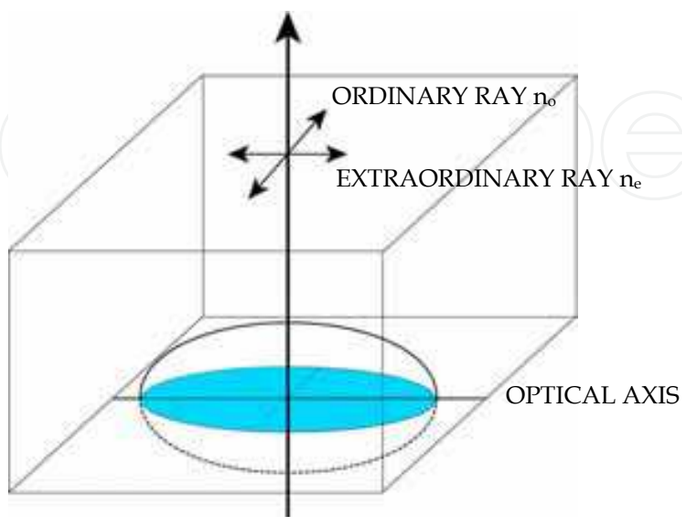

Fig. 19. Uniaxial crystal third example

These uniaxial crystals have tetragonal, rhombohedra and hexagonal cell.

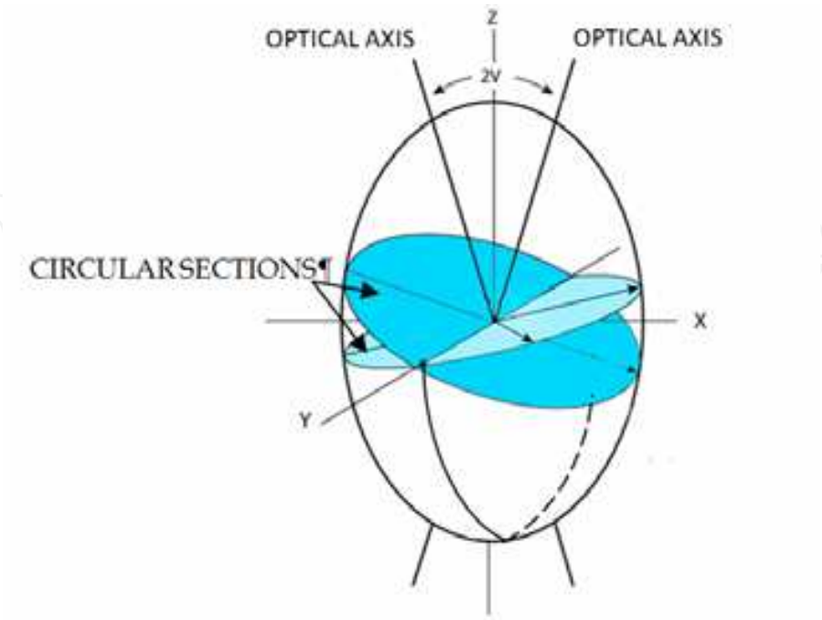

Fig. 20. Optical indicatrix for biaxial crystals

Those crystals having orthorhombic, monoclinic e triclinic cells are biaxial crystals. They have three different principal indices of refraction n_x, n_y and n_z, so that the indicatrix becomes a triaxial ellipsoid. Assuming that $n_x < n_y < n_z$, ZX plane is the optical plane and the Y axis is the optical normal (see fig. 20).
Between the two optical axes an acute angle, 2V, is the optical angle. The bisector of such angle is the acute bisector Bxa (see fig. 21): in the positive crystal that is Z axis, while in negative ones that is the X axis. The bisector of the other obtuse angle between the optical axes is the obtuse bisector Bxo.

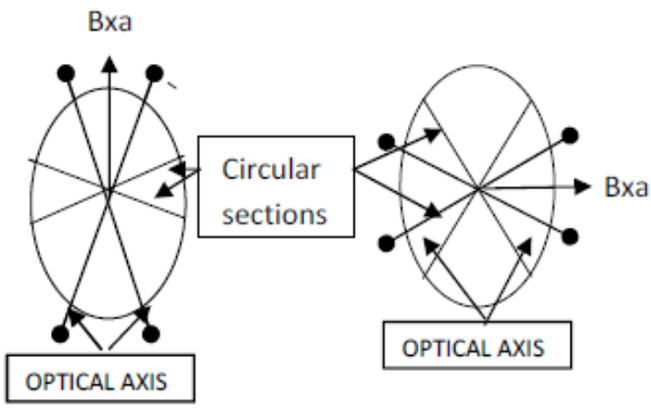

Fig. 21. Optical indicatrix for biaxial positive and negative crystals

The study of birefringence in this type of crystal can be conducted as in the case of uniaxial crystals. The indicatrix has the property that the axial sections normal to the optical axes are

circular with a radius equal to n_y: then, a wave that propagates along the optical axis will behave as if they were moving in an isotropic medium. Any other section is elliptical wave moving along a direction different from the optical axis, therefore, will split into two beams, with vibration directions parallel to the major and minor semi-axis of the ellipse. The optical angle can be determined experimentally, but there are approximated formulas for its calculation according to the value of the indices of refraction:

$$tg^2V = \frac{\frac{1}{n_x^2} - \frac{1}{n_y^2}}{\frac{1}{n_y^2} - \frac{1}{n_z^2}} \tag{23}$$

The eq. (23) is valid for Z axis bisector: if V > 45° the crystal is negative, while if V < 45° the crystal is positive.

4.2 Photoelasticity

Photoelasticity is a classical technique that allows to visualize internal stress/strain states in transparent materials; it exploits the changes in refractive indices induced by strain within transparent materials

4.2.1 General scheme of polariscope

The polariscope is an optical instrument which utilizes polarized light in inspecting a specimen subject to strain; usually it is used to explore a two-dimensional planar stress state, with stress components orthogonal to the optical axis *z*. Light travels across the material of the specimen and its polarization state is affected by the spatial distribution of refraction index, which depends on strain. According to the kind of polarization, it is possible to consider a *plane polariscope* or a *circular polariscope*.

In a plane polariscope, devices known as *plane or linear polarizer* are utilized: they are optical elements which divide an incident electromagnetic wave in two components which are mutually perpendicular (fig. 22). The component, which is parallel to the polarization axis is transmitted, while the perpendicular one is absorbed or totally reflected internally.

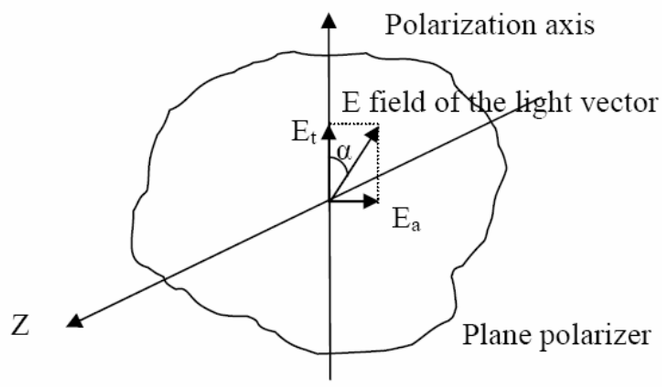

Fig. 22. Plane polarizer

It is possible to make the assumption that the polarizer is placed at the z_0 coordinate along the z axis, the equation of the light vector can be written:

$$E = a\cos\frac{2\pi}{\lambda}(z_0 - ct) \tag{24}$$

Since the initial phase is not important for this treatment, it is possible to rewrite it in the following way (it is assumed that $f = c/\lambda$ = wave frequency)

$$E = a\cos 2\pi ft = a\cos \omega t \tag{25}$$

where $\omega = 2\pi f$ is the wave angular frequency. The absorbed and transmitted components of light vector are:

$$E_a = a\cos\omega t\sin\alpha \quad E_t = a\cos\omega t\cos\alpha \tag{26}$$

where α is the angle between the light vector and the polarization axis.
In the plane polariscope two linear polarizers are used. Between those ones, the crystal under inspection is placed: the linear polarizer which is close to the light source is called the "*polarizer*", while that one placed on the opposite side with respect to the crystal is called the "*analyser*".

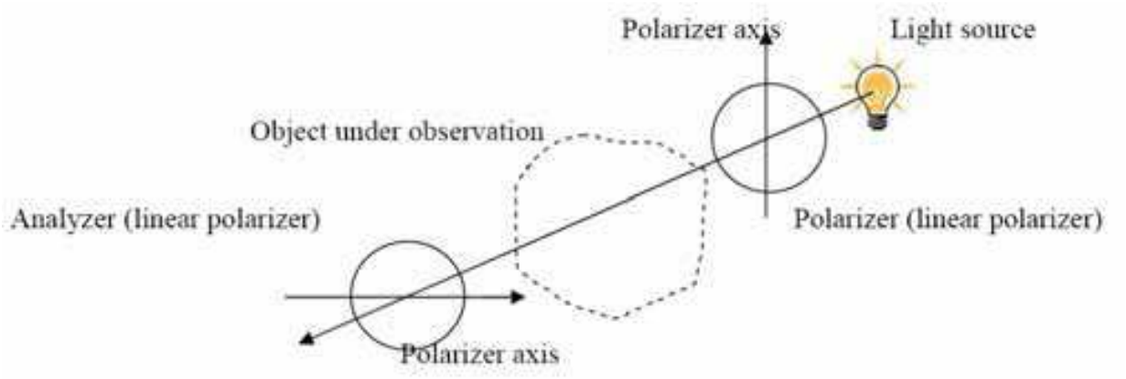

Fig. 23. Plane polariscope scheme

The usual configuration is the one where the two axes of polarization of analyser and polarizer are orthogonal to each other. The specimen to be analysed is put between the two, so that light goes through it. If the specimen is optically anisotropic, then light polarization is affected (see fig. 23). In our case the sample will be a crystal cut with plane surfaces. The advantage of such configuration is that what is observed is totally due to the crystal lattice effect: in fact, without crystal, light reaches the analyser could not be transmitted due to its perpendicular polarization with respect to the analyser polarization axis. Indeed this condition is also named "dark field". On the other hand, when a crystal is introduced, the crystal birefringence produces a light vector rotation of each light wave so that part of the light can pass the analyser.
In the circular polarizer (and in general in the elliptical one), a *wave plate* is used: it divides the light vector in two orthogonal components at different velocities. Such plate is produced with birefringence materials (Dally & Riley, 1987; Wood, 1964). The wave plate has two

principal axes, identified with number 1 and 2 (fig. 24): the transmission of the polarized light along the axis 1 occurs with the velocity c_1, while that one along the axis 2 occurs at c_2. In general $c_1 > c_2$, for this reason the axis 1 is the *fast axis*, while the axis 2 is the *slow axis*.

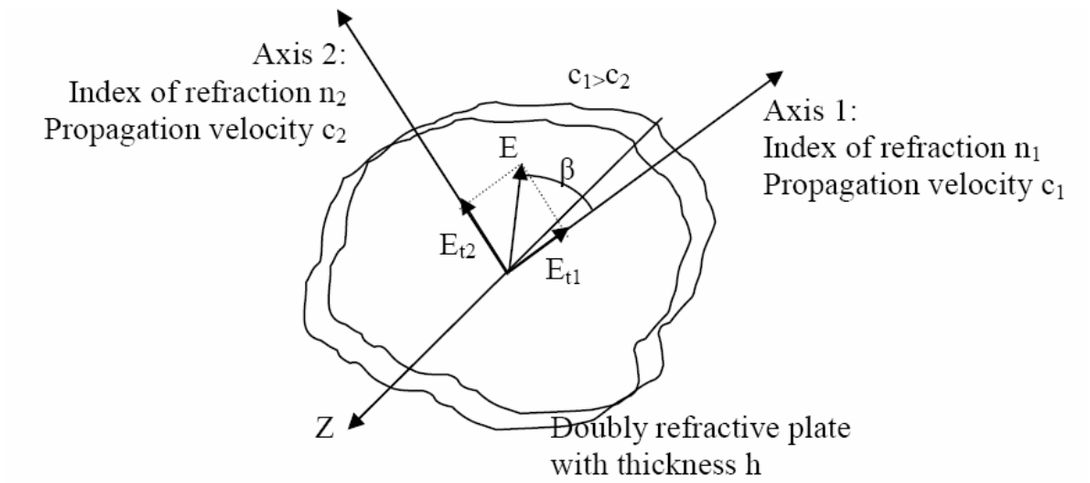

Fig. 24. Optical scheme of a wave plate

If a wave plate is placed after a polarizer, it is necessary to consider that the transmitted wave vector E_t forms an angle β with the fast axis 1. After that it has passed through the plate, E_t is divided in two components E_{t1} and E_{t2}, which are parallel respectively to 1 and 2 axis. The amplitudes of each resulting vector are:

$$\begin{aligned} E_{t1} &= E_t \cos\beta = a\cos\alpha\cos\omega t\cos\beta = k\cos\omega t\cos\beta \\ E_{t2} &= E_t \sin\beta = a\cos\alpha\cos\omega t\sin\beta = k\cos\omega t\sin\beta \end{aligned} \tag{27}$$

Where $k = a\cos\alpha$. Since the two components travel with different velocities (c_1 and c_2), they cross the plate at different times, implying a relative phase offset. Considering h the plate thickness, the relative delay, that both the wave, travelling across the plate, have with respect to a wave travelling in air (n is considered the air index of refraction), is respectively:

$$\delta_1 = h(n_1 - n) \qquad \delta_2 = h(n_2 - n)$$

And then the phase difference is

$$\delta = \delta_2 - \delta_1 = h(n_2 - n_1)$$

The angular phase difference Δ results:

$$\Delta = \frac{2\pi}{\lambda}\delta = \frac{2\pi h}{\lambda}(n_2 - n_1) \tag{28}$$

When $\Delta = \pi/2$ the wave plate is called a quarter wave plate (*λ/4)*. Once the two waves have abandoned the plate, they can be described by the following equations:

$$\begin{aligned} E_{t1}' &= k\cos\beta\cos\omega t \\ E_{t2}' &= k\sin\beta\cos(\omega t - \Delta) \end{aligned} \tag{29}$$

Recombining the two waves, the amplitude of the resulting wave vector considering these two components is expressed as following:

$$E_t^{'} = \sqrt{(E_{t1}^{'})^2 + (E_{t2}^{'})^2} = k\sqrt{\cos^2\beta\cos^2\omega t + \sin^2\beta\cos^2(\omega t - \Delta)} \tag{30}$$

The angle with respect to the axis 1 of the plate is:

$$\tan\gamma = \frac{E_{t2}^{'}}{E_{t1}^{'}} = \frac{\cos(\omega t - \Delta)}{\cos\omega t}\tan\beta \tag{31}$$

In order to obtain a circular polarization the λ/4 plates are used, with β equal to π/4. In this configuration it is possible to write:

$$E_t^{'} = \frac{\sqrt{2}}{2}k\sqrt{\cos^2\omega t + \sin^2\omega t} = \frac{\sqrt{2}}{2}k \tag{32}$$

$$\gamma = \omega t$$

It is possible to observe that the amplitude of the light vector is constant, while its direction (which is indicated by the angle γ with axis 1 of the plate) varies linearly with time: therefore, the tip of the vector forms a circle. In particular, if β = π/4 the rotation is counter-clockwise, while if β = 3π/4 the rotation is clockwise. In order to obtain an elliptic polarization a λ/4 plate is used oriented in such way that β ≠ nπ/4 (with n integer). It is possible to have:

$$E_t^{'} = k\sqrt{\cos^2\beta\cos^2\varpi t + \sin^2\beta\sin^2\varpi t} \tag{33}$$

$$\tan\gamma = \tan\beta\tan\varpi t$$

therefore, the tip of the light vector forms an ellipse. In general, λ/4 plate is used in order to obtain the circular polariscope see Fig. 25.

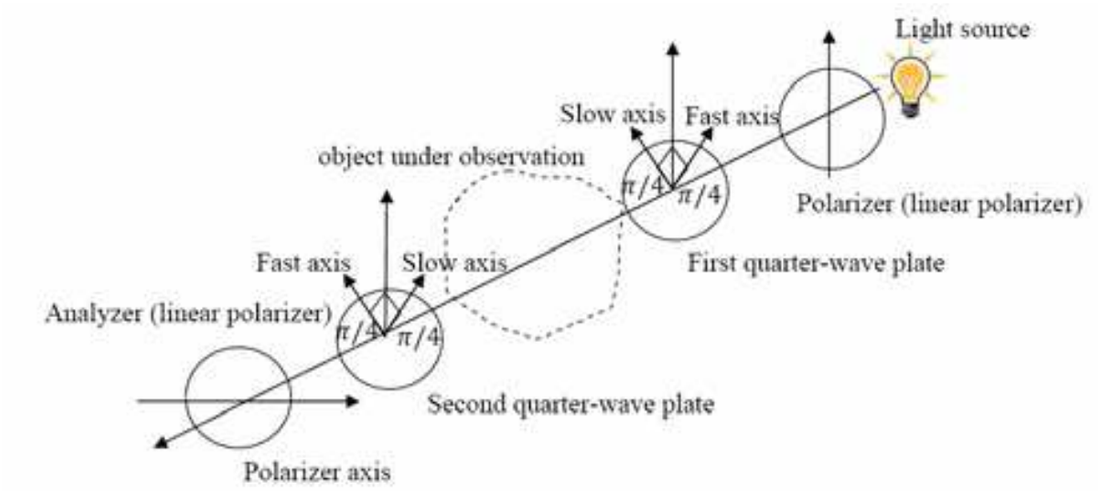

Fig. 25. Circular polariscope scheme

The first element is the polarizer which converts light in linearly polarized light with vertical direction. Then there is the $\lambda/4$ plate which is placed with an angle $\beta = \pi/4$ with respect to the polarization axis of the polarizer. In this way light undergoes circular polarization. Another $\lambda/4$ plate is place with the fast axis parallel to the slow axis of the previous one: the task is to convert the circular polarization in linear one with vertical direction. As last element, there is the analyzer with horizontal polarization axis which produces the dark field. The presence of the crystal between the two $\lambda/4$ plates let light pass through the analyser. In this way it is possible to observe interference fringes.
The interference figures belong to two families: isochromatics and isogyres. Intercepting the light coming from the analyser of the polariscope with a screen or plane of the observer, the isochromatic curves represent the loci where all rays with the same difference in optical path strike on such plane, while interference figure where the light vibration directions through the specimen are parallel to the polarization directions of polariscope are the isogyres.

4.3 Photoelasticity for quality control of crystal samples

The use of photoelastic techniques for quality control involves a knowledge of the piezo-optical properties of the crystal. As a matter of fact, the number of parameters concerning the piezo-optical effect, as far as refraction index variation cannot be directly calculated without the piezo-optic matrix Π, that relates stress and refraction indices. The components of the piezo-optic matrix Π depend on the symmetry group for each crystal (Nye, 1985, Sirotin et al., 1982). Due to the complexity of the three-dimensional problem of piezo-optic response of scintillating crystals, the values of the single components of Π, at present, are unknown for most crystals (to our best knowledge); therefore the procedure presented hereafter is essentially a semi-emipirical approach, which provides qualitative information and an integral indicator of the internal stress state which we call a quality index. It is not an accurate measurement of internal stress distribution, but nevertheless provides useful information for assessing if residual stress state developed in the crystal has reached critical values.
The methodology for quality control of the internal stress in scintillating crystals has been developed and demonstrated on the uniaxial $PbWO_4$ (PWO) crystal, but it can be extended to the whole class of uniaxial crystals. (PWO) is an optically uniaxial birefringent crystal with ordinary and extraordinary refraction indices $n_o = 2.234$ and $n_e = 2.163$ respectively, for $\lambda = 632.8$ nm (Baccaro et al., 1997). The development has been carried out on long prismatic samples, cut from an ingot and polished. They can be represented in a (x,y,z) Cartesian coordinate reference system with a solid body having rectangular cross-section (in the x-z plane) and length L (along y axis). The crystallographic c axis coincides with the optical axis (Born & Wolf, 1975; Walhstrom E., 1960), in a stress-free condition, that in the (x,y,z) reference coincides with the z axis. This is also the observation direction.
When the crystal sample is subjected to a uniform monoaxial compressive stress σ_y, this compressive stress induces the crystal to became biaxial, and, following the classical interference theory concerning anisotropic crystals, as stated by Born and Wolf (Born & Wolf, 1975), applied to bi-axial crystals, it can be found a fourth-order polynomial expression (34). Eq. 34 (Rinaldi et al., 2009) represents a model for the loci of the interference surfaces called the Bertin surfaces (Walhstrom, 1960):

$$(N\lambda)^2 = \left(x^2+y^2+z^2\right)\cdot(n_x-n_z)^2\left(1-\left[\frac{z\cdot\cos\beta+x\cdot\sin\beta}{\sqrt{x^2+y^2+z^2}}\right]^2\right)\cdot\left(1-\left[\frac{z\cdot\cos\beta-x\cdot\sin\beta}{\sqrt{x^2+y^2+z^2}}\right]^2\right) \quad (34)$$

where n_x, n_z are the refraction indices along the x and z axes, N is the fringe order, λ is the light wavelength of the light source for the observations, β is the semi-angle between the two optical axes when the crystal becomes biaxial under stress. β is represented by the following function of the three refraction indices n_x, n_y, n_z (Walhstrom E., 1960). Equation (35) holds for negative crystals (i.e. $n_e < n_o$) like PWO is (Walhstrom, 1960).

$$\tan^2\beta = \frac{\frac{1}{n_y^2}-\frac{1}{n_x^2}}{\frac{1}{n_z^2}-\frac{1}{n_y^2}} \quad (35)$$

For a sample of fixed thickness, equation (34) represents interference images given by "Cassini-like" 4th-order curves in the x-y plane. From equation (34) it can be obtained a family of fringes (isochromatic) that are parameterized by the fringe order N. Attention can be focussed on the first-order fringe (N = 1), as visible in a dark-field configuration of the plane polariscope (i.e. analyser perpendicular to laser polarisation). From a phenomenological point of view, supported by experiment evidence, it can be observed a linear dependence of the refraction index n_y on the applied stress σ, along the direction of application, at least for low stress levels. As a matter of fact, an applied stress along y affects all three refraction indices and the refraction index variations depends on the tensor ΔB (variation of dielectric impermeability) as expressed the matrix equation:

$$\begin{Bmatrix}\Delta B_{xx}\\ \Delta B_{yy}\\ \Delta B_{zz}\\ \Delta B_{xz}\\ \Delta B_{yz}\\ \Delta B_{xy}\end{Bmatrix} = \begin{bmatrix}\pi_{xxxx} & \pi_{xxyy} & \pi_{xxzz} & 0 & 0 & \pi_{xxxy}\\ \pi_{xxyy} & \pi_{xxxx} & \pi_{xxzz} & 0 & 0 & -\pi_{xxxy}\\ \pi_{zzxx} & \pi_{zzxx} & \pi_{zzzz} & 0 & 0 & 0\\ 0 & 0 & 0 & \pi_{xzxz} & \pi_{xzyz} & 0\\ 0 & 0 & 0 & -\pi_{xzyz} & \pi_{xzxz} & 0\\ \pi_{xyxx} & -\pi_{xyxx} & 0 & 0 & 0 & \pi_{xyxy}\end{bmatrix}\begin{Bmatrix}\sigma_{xx}\\ \sigma_{yy}\\ \sigma_{zz}\\ \sigma_{xz}\\ \sigma_{yz}\\ \sigma_{xy}\end{Bmatrix} \quad (36)$$

where the Voigt notation is used, and the Π components depend on 4/m point group symmetry concerning the PWO (Nye, 1985, Sirotin et al., 1982).
The dielectric tensor [ε] is obtained by the relation:

$$[B] = [B_0] + [\Delta B] = [\varepsilon]^{-1} \quad (37)$$

In a principal reference system, the refractive indices *n* can then be derived by:

$$n_i = \sqrt{\varepsilon_i}$$

Numerical simulations, based only on the variation of tanβ (eq.35) in equation (eq.34), produce results in agreement with the experimental observation in calculating the

isochromatic interference fringes. Therefore it appears a possibility to relate internal stress state to fringe geometry; the quality control methods developed are based on this experimental evidence, supported by theory. The interference images in the case of stress free uniaxial samples are families of circles. An applied load on the crystal sample induces a distortion that in the simple uniaxial stress case is a Cassini-like curve (Rinaldi et al., 2009), as the crystal becomes biaxial owing to the applied stress. For low stress level, these curves resembles ellipses.

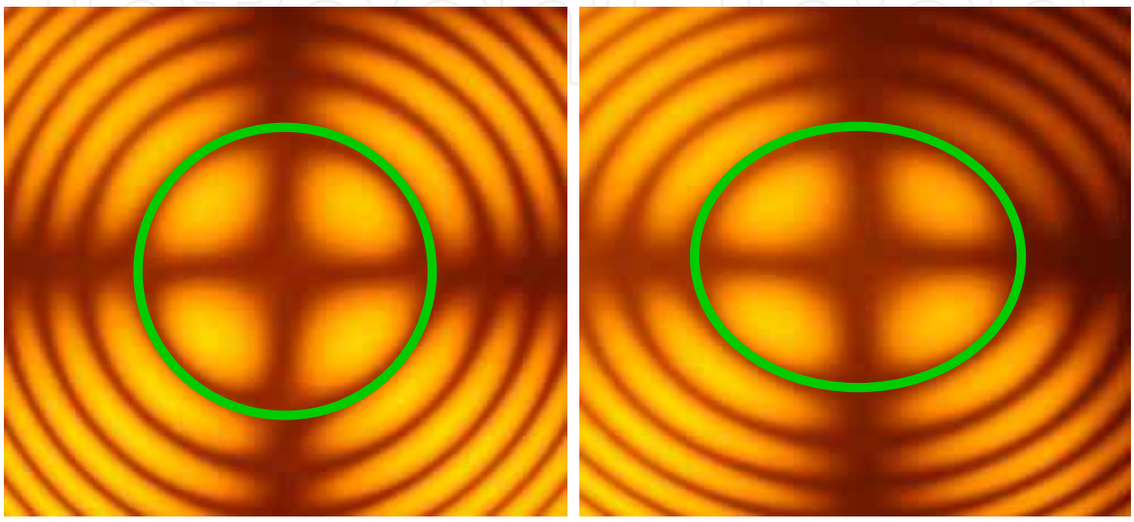

Fig. 26. PWO interference images. The highlighted first order fringe is fitted by the model from eq. 34. On the left, the crystal is stress free, on the right, it is subjected to a uniform, uniaxial compressive stress

Since the evaluation of the refraction index variations by means of (eq. 36) is a hard task, owing to the lack in the knowledge of the Π matrix, an alternative option is to evaluate the fringe distortion by means of an experimental index correlated to fringe distortion; to this purpose it was defined an elliptical ratio C_{ell} (Cocozzella N. et al., 2001) as:

$$C_{ell} = \frac{a}{b} - 1 \tag{38}$$

where a and b are the major and minor axes (along x and y respectively) of the first order isochromatic fringe obtained by observing the crystal in a plane polariscope in dark field (fig. 27). Therefore, in an empirical way, it is established a link between internal stress and fringe distortions by defining the photoelastic constant f_σ (Cocozzella N. et al., 2001) as:

$$\sigma_y \cdot f_\sigma = C_{ell} \tag{39}$$

In a series of works (Cocozzella N. et al., 2001; Lebau M. et al., 2005), it was experimentally verified in PWO samples that f_σ is a constant for a sample with thickness z = d, as C_{ell} depends linearly on σ_y. So it is necessary to systematically evaluate f_σ for PWO samples with different thicknesses d to relate (eq. 39) with the parameter d. Once this photoelastic parameter is known by calibration, which means experimental loading of a crystal sample

with known loads, then the same parameter can be used on unloaded samples to assess if an internal stress state is present; the amount of distorsion of the isochromatic fringe provides an empirical assessment on the existence of internal stress.

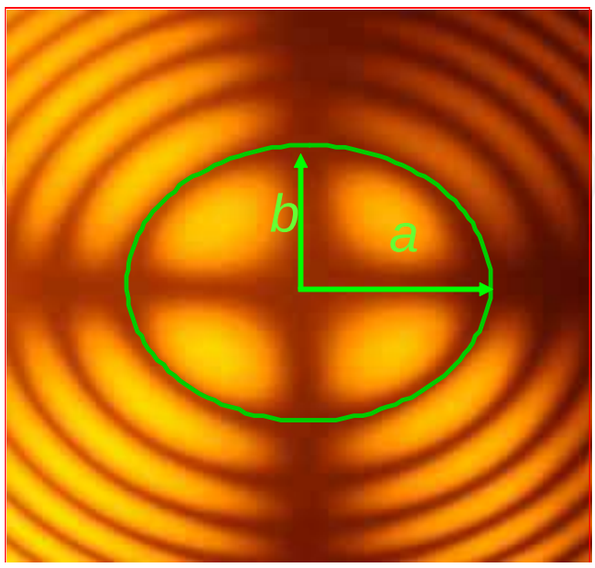

Fig. 27. Parameters used to define the elliptical ratio

In order to know f_σ as a function of d it is necessary to have a set of good quality PWO samples to which a known uniaxial load has to applied. This procedure was described in (Davì & Tiero, 1994); in that case samples have been chosen respecting the "De Saint Venant" conditions with thickness ranges from 5 to 15 mm and a dedicated compression loading machine was used. A dedicated polariscope employing a He-Ne laser source (λ = 632.8 nm) to perform the quality control tests can be designed (fig. 28) according to the classical polariscope theory (Born M., 1975).

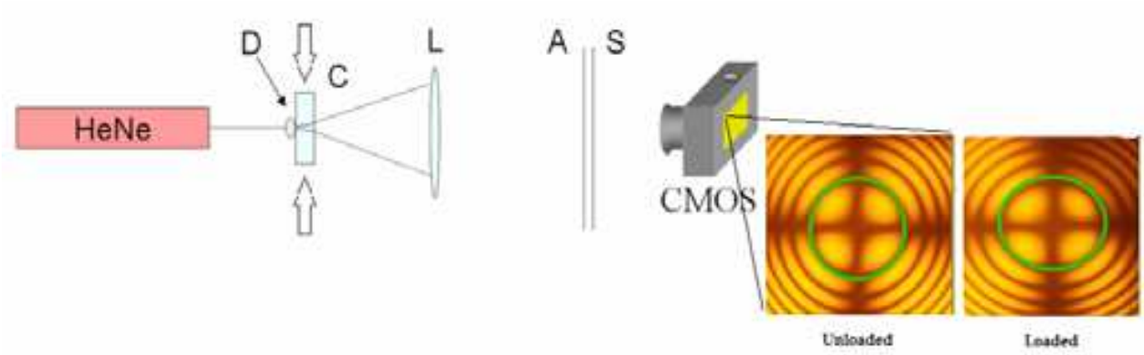

Fig. 28. Laser-light plane polariscope. In the dark field configuration, the analyser is set perpendicular to the light polarisation. D = glass diffuser. C = sample. L = convergent lens. A = analyser. S = ground glass screen

Some changes must be introduced when using laser source instead of a non-coherent diffused light source with respect of classical polariscope (Lebeau et al., 2005; Lebeau et al.,

2006; Frocht, 1941). As the laser light is already linearly polarized, the polarizer is not required. Moreover, interference fringes are obtained in convergent light so a small ground-glass diffuser was positioned just before the sample. Finally, all the parallel rays emerging from the crystal are focused on a ground glass screen, creating a bijective correspondence between the propagation direction inside the crystal and a point on the screen (Born & Wolf., 1975). C_{ell} is systematically measured versus f_σ applying uniaxial stresses along the y axis crystals, for different thicknesses of the PWO samples. All measured C_{ell} values exhibit a linear trend with the stress σ in the loading range 0-4 MPa. Four cases are reported in figure 29.

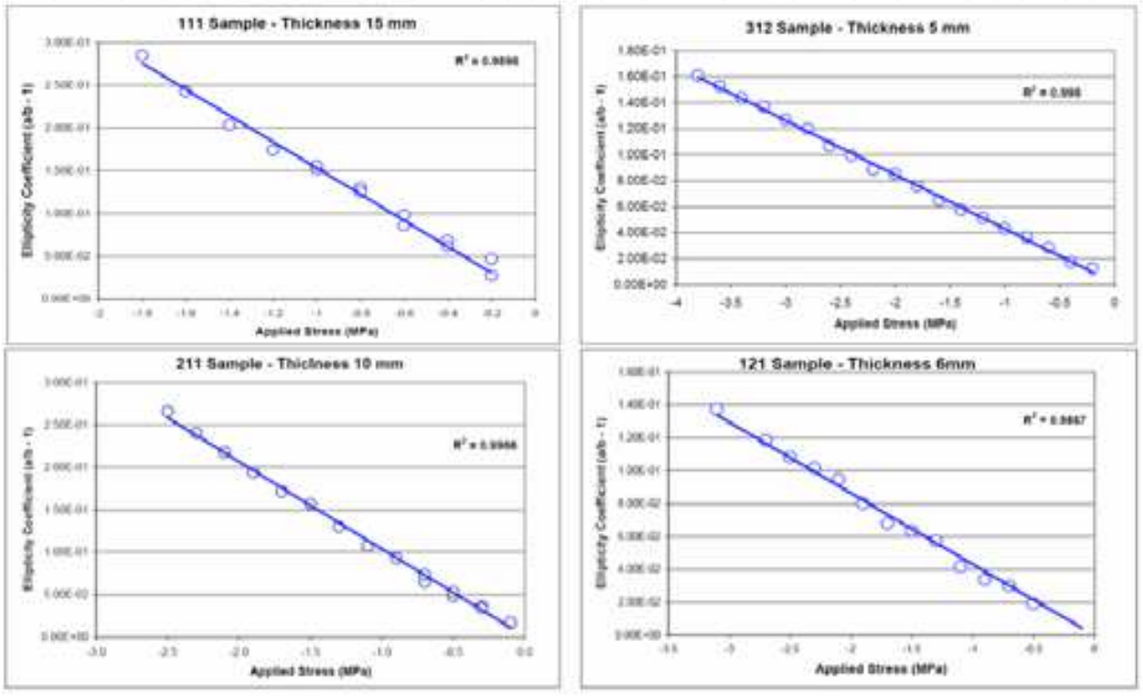

Fig. 29. The elliptical ratio C_{ell} as a function of applied stress for the four samples of different thickness

Numerical simulations, based on equation (34), and experimental data confirm that, C_{ell} linearly scales with the thickness. The resulting f_σ must also follow a linear dependence on crystal thickness z. The experimental data obtained using a laser with wavelength λ = 632.8 nm, lead to the evaluation of f_σ through a linear regression (correlation coefficient R = 0.997):

$$f_\sigma = 0.0172(\pm 0.0049) - 0.0114(\pm 0.0005)\, z \tag{40}$$

Numerical simulations from equations (eqs. 34 – 40), using realistic values of n_x, n_y, n_z, confirm the linear behaviour of f_σ versus z at least for z value not too close to z = 0 (for z=0 the analysis loose physical meaning) and for z lower than 20 mm. For larger samples (up to 30 mm), only simulations have been performed , in this case a second-order law rules the variation of f_σ versus z. For z ranging from 5 to 15 mm the linear law can be applied (Ciriaco et al., 2007).

4.3.1 Mapping residual stress distribution in a crystal boule

The knowledge of the photoelastic constant f_σ allows the evaluation of the internal stresses for PWO samples by means of the determination of the elliptical ratio, observing the crystals by means of plane polariscope using the same light length. The residual stresses developed during crystal growth tend to increase proportionally to the boule diameter, due to the thermal gradients resulting from growth conditions. The presence of residual stress can hardly be solved by process control. The knowledge of the stress distribution inside the sample during or after growth, can be used as a quality control technique and provide feed-back for growth process optimization; furthermore, it can address useful information for planning the mechanical processing.

In order to prove this concept, PWO samples have been studied by the photoelastic method explained above. For each sample, it is therefore determined the ellipticity coefficient C_{ell} of the first isochromatic fringe and through the photoelastic constant it is derived a stress estimate by:

$$\sigma = C_{ell} / f_\sigma \tag{41}$$

The boule was grown using the Czochralski method, with optical axis orthogonal to the sample axis (fig. 30); 8 samples were cut from the boule, with reference to the X-Y-Z cartesian frame of the figure. The stress distribution has been mapped in the samples. at different locations (x,y,z).

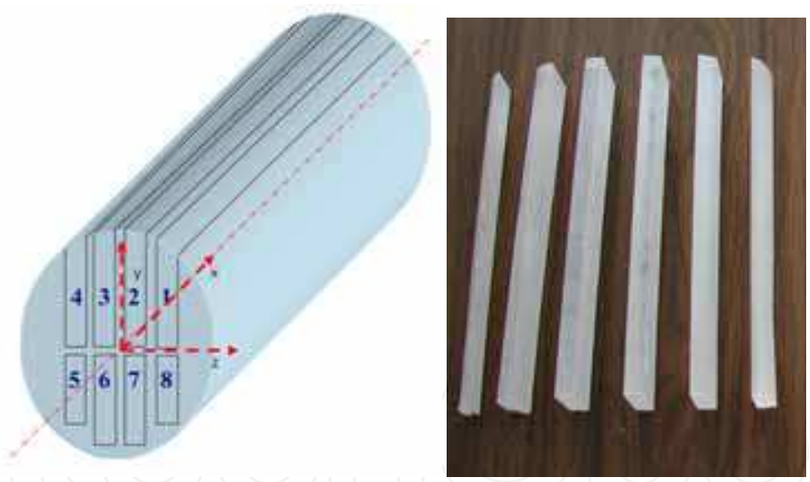

(a) (b)

Fig. 30. Samples position respect to the boule and reference axes (a); a photo of the 8 samples (b)

The mapping gives the possibility of the 3D recostruction of the stress distribution inside the boule; of course, one should taking into account that what observed is a stress state in the samples after cutting, therefore it represents the stress state after relaxation. If an appropriate model would be available, it could be possible to reconstruct the effective stress inside the boule after the growth before the cutting. In fig 31 the data for sample 2 are reported. From the overall data we can deduce that the stress decreases from seed to boule end. As expected, owing to delicate initial growth phase, the classical constant gradient distribution is due to high peripheral tension compared to low internal compression. It

should be noted that values are taken after the cutting off of crystal volume in a larger boule; this changes the internal stress state. The original tensional state is unknown and certainly can be higher because of stress relief from cutting. However, the method gives information about the growth of crystals that are fundamental to understanding the growth phenomenon and for the design of the production cycle. Therefore it provides a method for quality control and tuning of crystal production through the analysis of samples taken from the process.

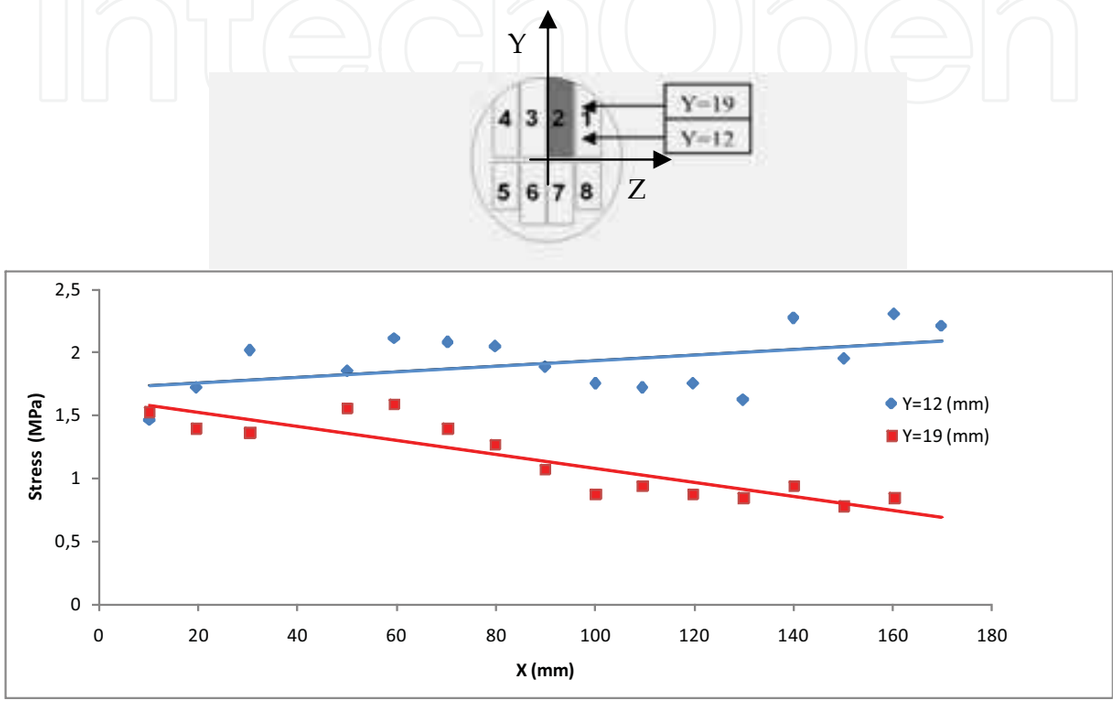

Fig. 31. Stress map inside the sample 2 as a function of sample length x, starting from the seed

A theoretical model of stress is needed in order to extrapolate the initial stress in the boule. Given this limit, this method allows for modifying and optimising the production process. It may lead to re-shaping the boule cone profile to obtain crystals with lower residual stresses. Moreover the obtained data pave the way to balance the process before and after annealing (stress-relief pre-cuts) and for appropriately sequencing the cutting operations, in order to reduce the losses by breaking.

4.3.2 Quality index

Given the characteristics of the quality control method presented above, it emerges that if a synthetic quality index would be available, the procedure could be helpful in tuning a production process.

It is worth to remark again that photoelasticity provides information about stress components in the plane normal to the polariscope axis, aligned in the direction of the optical axis. It is necessary to stress that what is observed, results from the effect of the principal stress difference absolute value, e.g. $|\sigma_{11}-\sigma_{22}|$, in the plane normal to the observation direction. So, we cannot measure, as a matter of fact, the value of each stress component. A single stress component is measured in the case of clearly monoaxial stress

field, as in the classical case of an imposed stress by a loading device (Rinaldi et al., 2009, Lebeau et al., 2005) In what follows, for convenience the expression stress-level has been used instead of the absolute principal stress difference. The reported analysis is applied to PWO, but can be extended to the overall family of similar uniaxial crystals. The family of circular isochromatic fringes are in a plane normal to the optical axis, in the case of unstressed crystals. Stress components contained in this plane induce a biaxial state and we detect a family of Cassini-like fringes as explained before, and following the protocol explained in this chapter , the internal stress level was computed from the measurement of the elliptical ratio.

The production of a large number of high quality crystals is a hard goal to perform owing to the complex production route involving different parameters to be controlled. For this, a quality control plan is needed. The need to produce while minimizing costs and production time, leads to the implementation of a fast and easy feed-back on growth parameters, such as temperature distribution and solidification-front velocity. In the following it is proposed a quality feedback for process optimization, obtained by a fast characterization of sample crystals taken from the pre-serial production using the photoelastic methods outlined above. For this purpose, it is possible to use also a classical plane polariscope (in alternative to the previous explained laser light polariscope). In the proposed analysis a green monochromatic light (λ = 530 nm) has been used.

Quality control dedicated to the selection of the better production process is made by taking crystals randomly extracted from every delivered batch.

In this example the ingots were produced by a "modified" Bridgman method: the platinum crucible has a 35x35 mm² section and is about 300 mm long. The fusion front temperature is controlled at 1250 (nominal) ± 0.5 °C. A slow and steady shift of the solidification front is produced by the movement of a thermal gradient estimated 30°C/cm at the solid-liquid interface. Using the Bridgman method, the optical axis is along the longitudinal axis, for this, each ingot was cut in 10 mm-thick slices, numbered starting from the seed as shown in fig. 32.

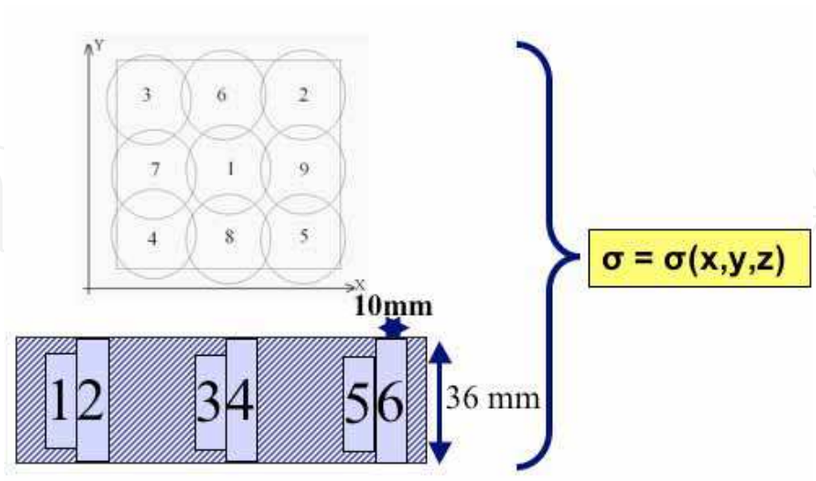

Fig. 32. Typical positions observed in each slice. Position 1 is called centre, positions 2-5 corner and position 6-9 "edge middle" (upper figure). Position of the slices cut normal to the crystallographic C-axis (optical axis) (lower figure)

The stress can be measured in typical locations in each slice, as is shown in Fig. 32. The cut of the slices orthogonal to the growth axis (Z), induces a stress relaxation in the axial components σ_z and in the shear stresses τ_{xz} and τ_{yz}.

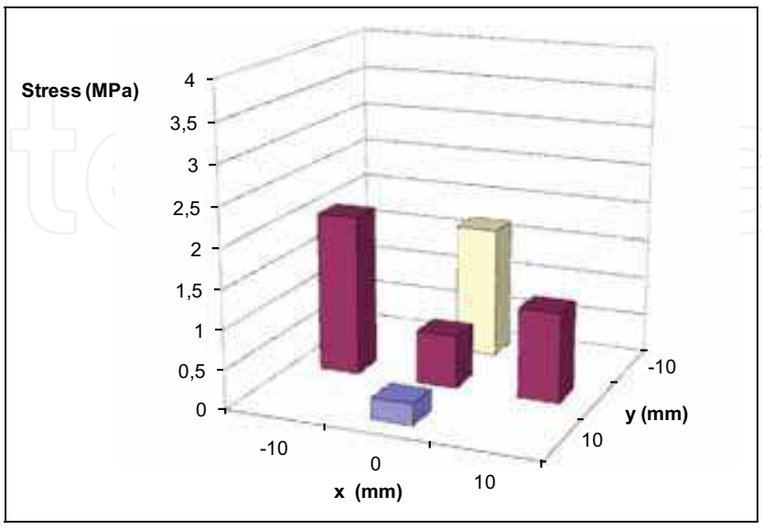

Fig. 33. Principal stress along x and y directions on slice 5

A 3-D reconstruction of stress distribution is possible staring from the measurements for each slice in the typical positions. The reported example leads to the following data (fig. 33, 34 and 35).

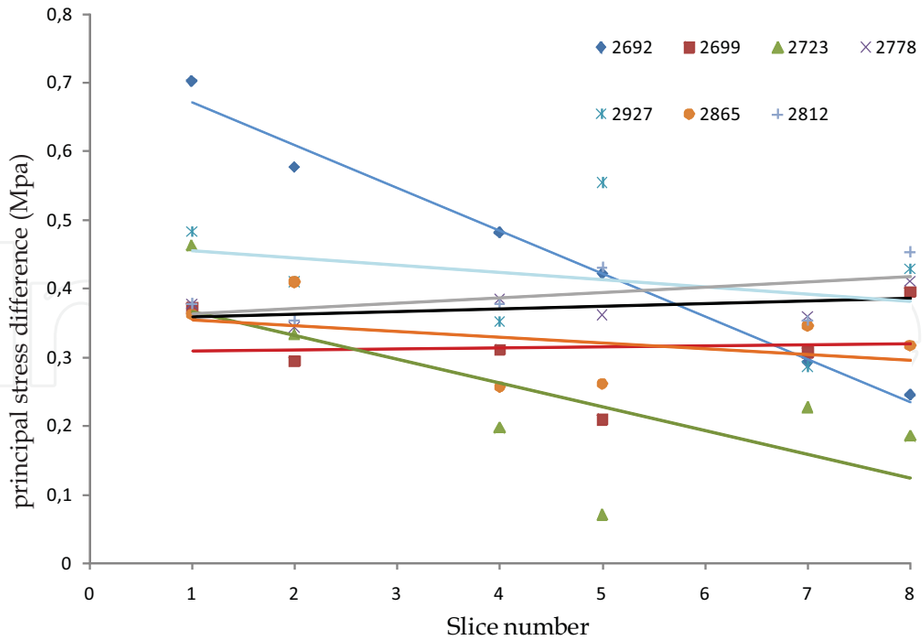

Fig. 34. Longitudinal average stress at slice corners for the 7 samples labeled in the figure. Generally decreasing trend from the seed to the end of crystal is confirmed. Linear regression have been shown for each crystal

The large stress difference at the corners for Sample 2692 in the first slice can suggest the presence of thermal problems after the solidification in the initial part or a crucible defect. The single crystal stress homogeneity seems to be restored at the crystal end. A not optimal thermal field displacement can also be supposed. The speed of temperature change could have been too high in the early growth stages of 2692 sample.

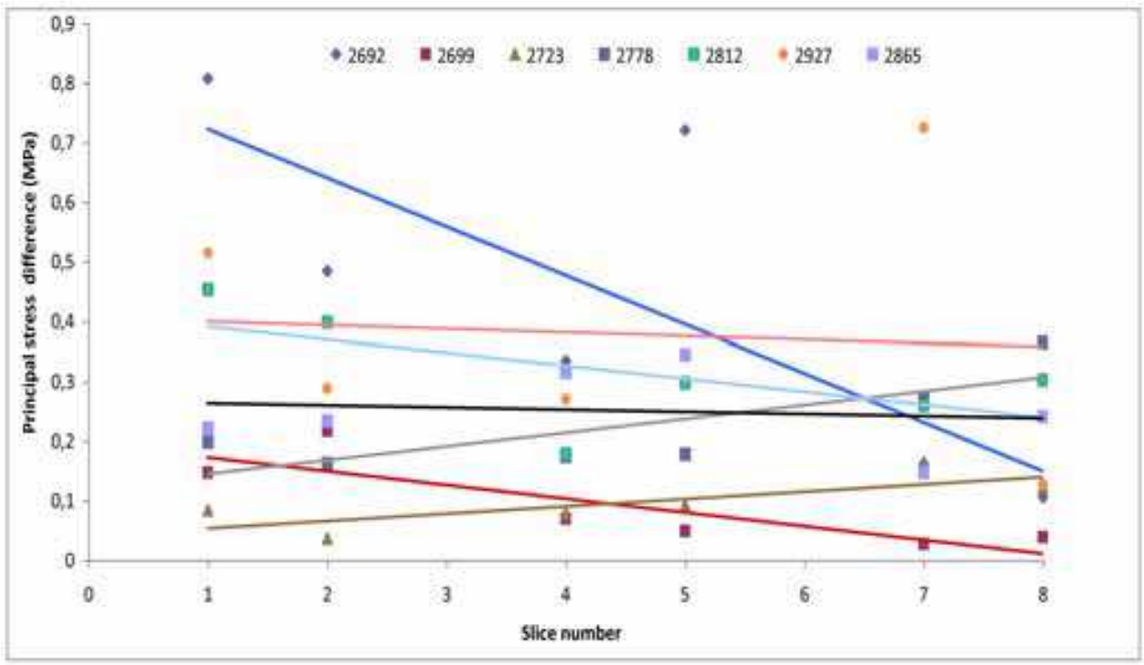

Fig. 35. Longitudinal trend at centre of the slices for the 7 samples labeled in the figure

The data collected can provide an analytical overview of the problem by assessing the evolution of stress in the mapping of the crystals. This analysis puts emphasis on individual problems that emerged during growth. The need of a synthetic index of quality derives from the necessity to understand what production parameters must be changed in the direction of better overall quality. The problem lies in handling a large quantity of data, as in the example shown. Extracting the average measures of stress from 6 samples we can write the following table:

SAMPLE	St. Dev. [MPa]	Mean [MPa]
2692	0.38	0.62
2699	0.38	0.36
2723	0.37	0.29
2778	0.33	0.54
2812	0.23	0.52
2865	0.33	0.39

Table 1. Mean stress and standard deviation of 6 samples

Quality control dedicated to the selection of the better production process is made by taking crystals randomly selected from every delivered batch. A large set of data can be collected from ingots produced in different conditions.
The residual stress inside the crystals can vary heavily depending on the type of process used but also as a function of the position inside the crystal.
In order to identify the best method of production and to guide the development of production methods, it's necessary to find a summary measure of the quality of the samples. To evaluate in synthetic manner the overall quality of each crystal, the data can be put in a Cartesian plane, with X axis the average stress level (σ_{av}) of all the measured points from each ingot, and Y axis the corresponding standard deviation (S). It is possible to define an "index of quality", R (Rinaldi et al., 2010):

$$R = \sqrt{(kS)^2 + \sigma_{av}^2} \tag{42}$$

In brittle materials, as in particular single crystals, the stress level variation may cause breaking risk, due to the gradient, as dangerous as the than an high average value σ_{av}. For this, larger values of R correspond to the lower crystal quality. The standard deviation S is weighted with a coefficient k (≥ 1) to be set from the producer in order to achieve the results identified on the basis of the required quality standards. k amplifies the standard deviation with respect to the average stress value highlighting the existence of gradients and inhomogeneity.
The general purpose of the (eq. 42) need some explanations linking the mathematical properties of (eq. 36) to the physical meaning of the parameters.
In the plane S-σ_{av}, the R=const. is a boundary delimiting an area related to the ingots quality. Each crystal is identified by its σ_{av} and S. The accepted crystals are in the area below the curve R=const. From the producer point of view, R will be the maximum σ_{av} acceptable (that is σ_M). Choosing k following the experimental experience and related to the quality, in terms of homogeneity required, it is easy to calculate the maximum S, that is $S_M = R/k = \sigma_M/k$. It is evident that the maximum standard deviation, S_M , must be lower than, or at least equal to the average stress level in the limit case. From the quality point of view the need that the stress variation must be controlled leads to a new constrain:

$$S = c\sigma_{av} \tag{43}$$

with c the slope of a line in the plane S-σ_{av}, c must be chosen for $c \leq 1$, as explained above. The acceptance area is below the curves. These constrains depend both from the average stress and the weighted stress standard deviation. The condition that the standard deviation cannot exceed the average stress value is thought fundamental in brittle materials, in fact, the stress variation, due to the crystal heterogeneity, might increase the breaking risk. In fig. 36 an example of this technique is shown.
The boundary curves delimiting the acceptability area are obtained with k = 1.5 and the limit quality value is R = 0,7 MPa. c = 1 was chosen as a limit case. These parameters can be set by the manufacturer according to statistical data of accidental cracking. Only two samples (highlighted by the blue oval) lie in the acceptability area, that is below the curves

42 and 43. The fact that three samples (2865, 2723 and 2699) are close to the line where standard deviation is equal to the average stress value clearly highlights the existence of high stress gradient. In particular the 2723 and 2699 samples are below the curve (eq. 42) but above the line (eq. 43), therefore are not accepted due to the high stress gradient. From this analysis it is possible to conclude that the process 2865 and 2812 have the best production parameter and indicates the development direction to improve the crystals quality. As final analysis it is possible to perform a comparison between the best and worst samples to put in evidence the specific critical points, as shown in the figure 37 (Rinaldi et al., 2010).

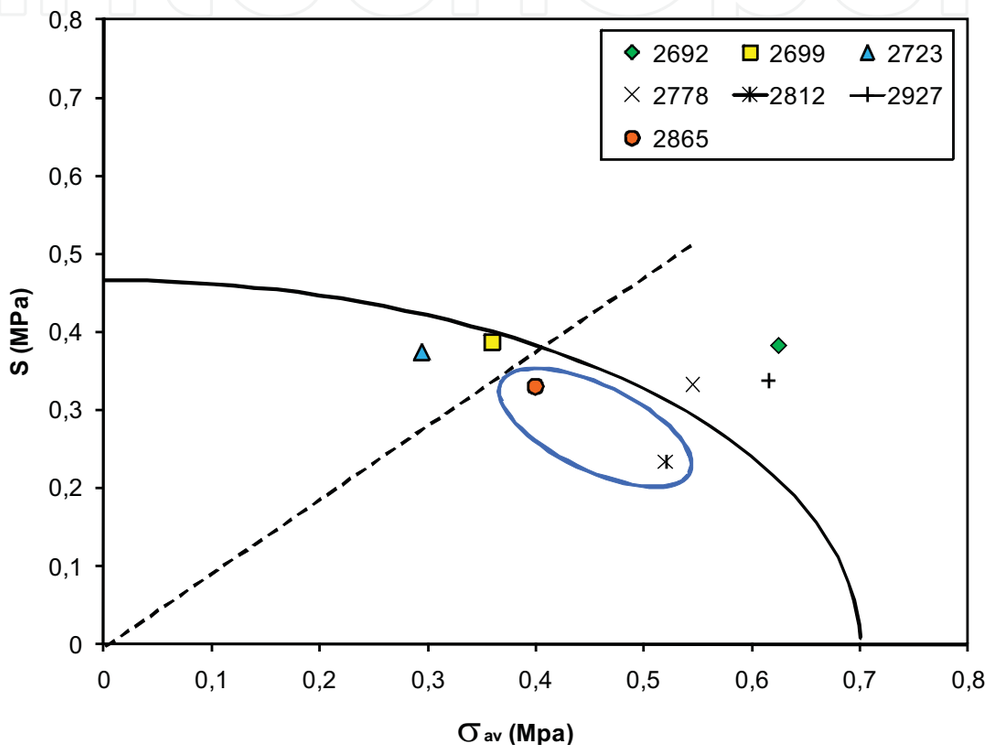

Fig. 36. Different samples in the plane S-σ_{av}. Only samples 2865 and 2812 are accepted, meeting the quality requirements

Fig. 37 clearly put in evidence that the low quality sample 2692 exhibits high absolute stress values but also high stress variation. On the other hand, the higher level quality sample 2865 has lower absolute stress values and it appears more homogenous. It indicates that the specific production process is well tuned and that probably the production parameter and gradients are well controlled yielding an homogeneous sample.

4. Conclusions

Scintillating crystals are widely used in radiographic systems, in computerized axial tomography devices and in calorimeter used in high energy physics. Scintillating crystals are cut to their final shape from an ingot, which is grown by classical crystal growth techniques. From a mechanical point of view, the quality of a crystal is closely related to its

geometry, to the surface finish and moreover to its internal state of residual stresses. In particular an excessive residual stress is a major cause of crystal breakage, which often may occur during crystal cut, during surface finishing or, even worse, only when the crystal is assembled into the detector units.

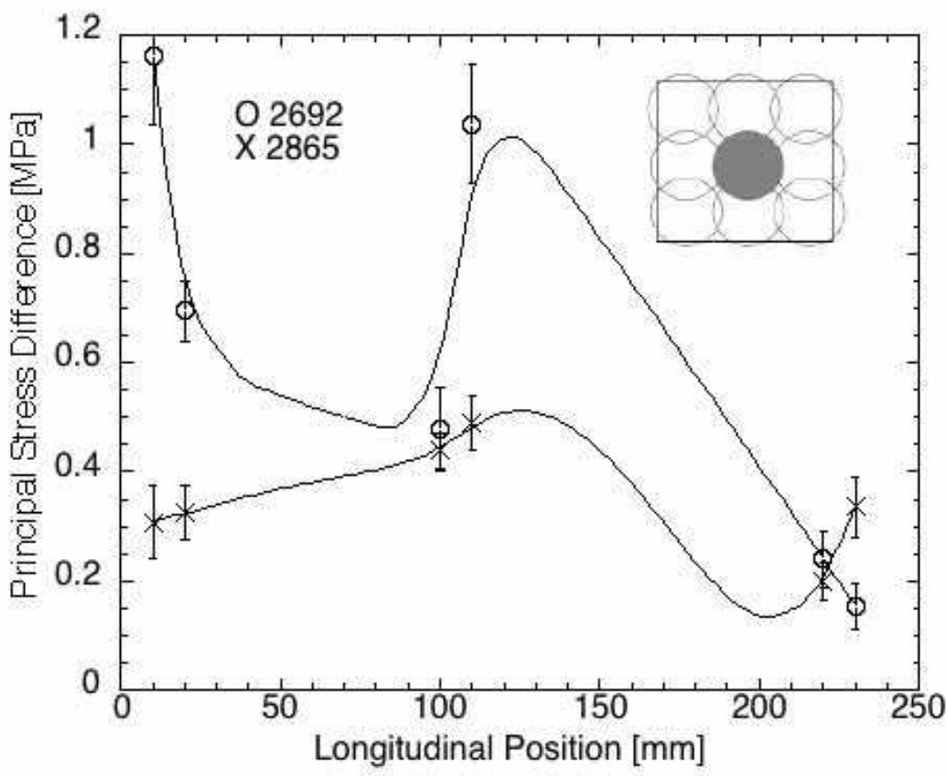

Fig. 37. Comparison between better/worst samples at centre position of the slices (as shown by the inset) as a function of the longitudinal position from the seed

The need to produce high-quality crystals is therefore fundamental both to avoid damage during assembly and finishing of crystals. Crystal performance in terms of production of light strongly depends on surface finish, therefore crystal tool machining is a crucial process to achieve the high performance needed in the case of scintillating crystals for high energy physics and medical applications.

For optimal crystals performance, attention has therefore to be paid to the mechanical aspects of the production process; from the mechanical point of view this can be guaranteed by adequate quality control methods. If adequate quality inspection of crystals is achieved, this has the potential to prevent breaking during the assembly in an array. The authors have reported the experience which was made within the collaboration with CERN to the development of the electromagnetic calorimeter of the Compact Muon Solenoid (CMS) presently working at CERN. From an industrial point of view, the trend is to use smaller and smaller crystals for biomedical instrumentation; in such crystals the surface plays an even more relevant role in the production of light. For this reason, the final mechanical processing is important for producing high quality crystals. Therefore the experience made for the large crystals of CMS is in general valuable to guide the

development of suitable quality control methods for scintillating crystals and in particular for biomedical industry.

An increasing attention to limit production costs requires an assessment of crystal quality by a fast and possibly non-destructive methodology, finalized to tune and keep under control the crystal growth and finishing processes, and to eliminate from the production process the crystals which are produced out of tolerance, thus reducing downtime and waste.

Internal residual stress is not only the most important causes of breaking, but may be interpreted as an overall quality indicator.

Residual stresses, induced by temperature spatial and temporal distribution during the growth and by complex interaction of the melt material and the growing ingot with the crucible, play an important role in production yield in terms of cracking risk during mechanical processing and heterogeneity in finished crystal properties. A regular production of good crystals requires a quality control plan leading to a fast and easy feed-back on growth parameters, such as temperature distribution and solidification-front velocity. The developed methodology for quality control consists in providing the producer a quality feedback for process control and optimization, obtained by experimental characterization of sample crystals taken from the pre-serial production by photoelasticity. Photoelasticity is a measurement technique aiming to study and evaluate the stress state inside a transparent medium. In traditional photoelasticity a plane stress state distribution is studied, by means of a plane polariscope. Usually it is applied to optically isotropic media, Perspex, glass or optically isotropic crystals, which become birefringent under stress.

Referring to naturally anisotropic media, such as uniaxial and biaxial scintillating crystals, the observation of unstressed crystals, by means of a plane polariscope, shows a symmetrical interference pattern due to the symmetry of the lattice. An internal stress state induces a lattice symmetry distortion. The modelling of the interference image obtained from an anisotropic uniaxial crystal when a stress state is present, and the measurement of characteristic parameters of the interference fringe pattern offers a mean for quality control able to provide spatially integrated information on the internal stress.

Although a mathematical modelling of the piezo-optical effects is possible, the knowledge of the coefficients of the model is not complete and accurate; therefore a semi-empirical approach is proposed. This leads to the definition of a parameter correlated to the deformation of the fringe pattern of a crystal under stress. The ellipticity, introduced into the fringe pattern is due to the stress state. Linear regression of experimental data of ellipticity vs. stress, collected with crystals undergoing known stress states, allows to build an experimental relationship which can then be used for quality assessment of unknown crystal samples. If the internal stresses are residual stresses, this allows to develop a quality control method to detect the presence of residual stresses non invasively. The method could be applicable on samples taken from the production, for process optimization and control, or it can be applied on the finished crystal as a pass-fail filter for removing from the batch all samples which exceed prescribed limits.

The statistical analysis of many data from samples randomly taken from a pre-serial production allows to build a quality index depending on mean stress value and on its standard deviation, which are quantities related to residual stress intensity and gradient. This index can be used as a global indicator of process capacity to produce crystals with acceptable residual stress state.

This method suggests therefore a quality indicator to synthetically evaluate the production by means of a criterion of acceptability, useful in general crystal production.
The procedure and the quality index have been validated on $PbWO_4$ (PWO) uniaxial scintillating crystals; they have been intensively studied owing to the necessity of large amount of them (about 82000 large crystals) for the CMS. In fact the production effort needed a fast and reliable quality control.
In that case study, the attention was focused on the measurement of residual stresses over the whole crystal volume, particularly in sections cut perpendicularly to the optical axis. The collected data enabled the construction of a 3-dimensional stress map for each crystal from a pre-serial production. The detection of internal stress and defects, can be related to the corresponding production parameters and may suggest improvements in the production process or highlight criticalities to be solved before a serial production is started.
What presented is demonstrated for uniaxial crystals, but the same approach can be extended to all types of crystals, particularly those of a new generation (LYSO, LuYAP) as a function of their applications in high energy physics and for medical diagnostics.
As conclusive remarks, we have to consider that other techniques should be taken into account to analyse crystals quality. In particular researchers are paying attention to experimental methods for the assessment of the surface damage, which are not treated in this chapter: X-ray diffraction (XRD), grazing incidence X-ray diffraction (GID) and RX reflectometry (XRR), (Mengucci et al., 2005).

5. Acknowledgment

This work has seen the contribution of many colleagues, amongst which we thank prof. Giuseppe Majni and Prof. Fabrizio Davì, who contributed through many fruitful discussions. A relevant part of the work has been developed with the direct contribution of students amongst which we warmly thank Nicola Cocozzella, who was the first to deal with this topic, and PhD candidates, in particular dr. Andrea Ciriaco, whose PhD thesis constitutes a milestone in our work.

6. References

Auffray E., Cavallari F., Lebeau M., Lecoq P., Schneegans M., Sempere-Roldan P. (2002). *Crystal conditioning for high-energy physics detectors*, Nuclear Instruments and Methods in Physics Research Section A (NIM A) 486, pp. 22-34.

Baccaro S., Barone L. M., Borgia B., Castelli F., Cavallari F., Dafinei I., de Notaristefani F., Diemoz M., Festinesi A., Leonardi E., Longo E., Montecchi M., Organtini G. (1997). *Ordinary and extraordinary complex refractive index of the lead tungstate ($PbWO_4$) crystal*. Nuclear Instruments and Methods in Physics Research Section A, 385, pp. 209-214.

Born M., Wolf E., (1975). *Principles Of Optics*, 6th ed., Pergamon press, New York, USA.

Cocozzella N., Lebeau M., Majni G., Paone N., Rinaldi D. (2001). *Quality inspection of anisotropic scintillating lead tungstate ($PbWO_4$) crystals through measurement of interferometric fringe pattern parameters*. Nuclear Instruments and Methods in Physics Research Section A (NIM A) 469 3 pp.331-339.

Ciriaco A., Davì F., Lebeau M., Majni G., Paone N., Pietroni P., Rinaldi D. (2007). *PWO photo-elastic parameter calibration by laser-based polariscope.* Nuclear Instruments and Methods in Physics Research A 570, 55–60

Dally J. W., Riley W. F., (1987). *Experimental Stress Analysis*, 2nd ed., McGraw-Hill Book Company, Singapore.

Davì F. and Tiero A., (1994). *The Saint-Venant's problem with Voigt's hypotheses for anisotropic solids*. J. Elasticity 36, pp. 183-199.

Frocht, M.M. *Photoelasticity*, Wiley, New York, 1941.

Hodgkinson I. J., Wu Q. H., (1997). *Birefringent Thin Films and Polarizing Elements*, World Scientific, New Jersey, USA.

Hofstadter, R (1949). *The detection of gamma-rays with thallium-activated sodium iodide crystals*. Phys.Rev. 75, pp. 796-810.

Ishii M., Kobayashi M. (1996). *Mechanical properties of PWO*. Nuclear Instruments and Methods in Physics Research Section A (NIM A) 376, pp. 203-207

Lebeau M. (1985). *Monocrystalline bismuth germanate $Bi_4Ge_3O_{12}$ (BGO) recent results on mechanical properties.* J.Mat.Sci.letters 4, 779-782.

Lebeau M., Ciriaco A., Gobbi L., Majni G., Paone N., Pietroni P., Rinaldi D. *Quality monitoring in PWO scintillating crystal production during R&D phase* Proceedings of the 8th International Conference on Inorganic Scintillators and their Use in Scientific and Industrial Applications, Publisher: National Academy of Sciences of Ukraine, Kharkov (2006) 334-337.

Lebeau M. (2003). Crystal Growth Technology. In *Methods and Tools for Mechanical Processing of Anisotropic Scintillating Crystals*, pp.561-586. Wiley and Sons, London.

Lebeau M., Pietroni P., Gobbi L., Majni G., Paone N., Rinaldi D. (2005). Mapping residual stresses in $PbWO_4$ crystals using photoelastic analysis., *Proceedings of Scint'03 7th International Conference on Inorganic Scintillators*, September 8-12, 2003, Valencia, Spain. NIM A537 154-158

Lecoq P. et al. (2006). *Inorganic Scintillators for Detector Systems*. ISBN-10 3-540-27766-8 Springer Berlin Heidelberg New York.

Mengucci P., Di Cristoforo A., Lebeau M., Majni G., Paone N., Pietroni P., Rinaldi D. (2005) *Surface quality inspection of $PbWO_4$ crystals by grazing incidence X-ray diffraction*. Nuclear Instruments and Methods in Physics Research Section A (NIM A) 537, 207-210.

Perelomova N. V. and Tagieva N. M., (1983). *Problems in Crystal Physics with solutions*, Mir Publishers, Moscow, Russia.

Pietroni P., Lebeau M., Majni G., Paone N., Rinaldi D. (2005). *Development of Young's modulus non-destructive measurement techniques in non-oriented CeF_3 crystals.* Nuclear Instruments and Methods in Physics Research Section A (NIM A) 537, 203-206.

Rinaldi D., Lebeau M., Majni G., Paone N. (1997). *Photoelasticity for the investigation of internal stress in BGO scintillating crystals*. Nuclear Instruments and Methods in Physics Research Section A (NIM A) 317-322.

Rinaldi D., P. Pietroni, F. Davì (2009). *Isochromate fringes simulation by Cassini-like curves for photoelastic analysis of birefringent crystals.* Nuclear Inst. and Methods in Physics Research, A 603, 294–300

Rinaldi D., Ciriaco A., Lebeau M., Paone N. (2010). *Quality control on pre-serial Bridgman production of $PbWO_4$ scintillating crystals by means of photoelasticity* Nuclear Inst. and Methods in Physics Research, A 615, 254–258

Walhstrom E.E., (1960). *Optical Crystallography*, Wiley, New York, (USA).

Weber M., Monchamp R. (1973). *Luminescence of $Bi_4Ge_3O_{12}$*- Journal of Applied Physics 44: 5495-5499.

Wood E. A. (1964). *Crystal And Light*, Van Nostrand Company, New Jersey.

Wooster, W. A. (1938). *A test-book on Crystal Physics*, Cambridge University Press.

Wide Spectra of Quality Control

Edited by Dr. Isin Akyar

ISBN 978-953-307-683-6
Hard cover, 532 pages
Publisher InTech
Published online 07, July, 2011
Published in print edition July, 2011

Quality control is a standard which certainly has become a style of living. With the improvement of technology every day, we meet new and complicated devices and methods in different fields. Quality control explains the directed use of testing to measure the achievement of a specific standard. It is the process, procedures and authority used to accept or reject all components, drug product containers, closures, in-process materials, packaging material, labeling and drug products, and the authority to review production records to assure that no errors have occurred.The quality which is supposed to be achieved is not a concept which can be controlled by easy, numerical or other means, but it is the control over the intrinsic quality of a test facility and its studies. The aim of this book is to share useful and practical knowledge about quality control in several fields with the people who want to improve their knowledge.

InTech Europe
University Campus STeP Ri
Slavka Krautzeka 83/A
51000 Rijeka, Croatia
Phone: +385 (51) 770 447
Fax: +385 (51) 686 166
www.intechopen.com

InTech China
Unit 405, Office Block, Hotel Equatorial Shanghai
No.65, Yan An Road (West), Shanghai, 200040, China
中国上海市延安西路65号上海国际贵都大饭店办公楼405单元
Phone: +86-21-62489820
Fax: +86-21-62489821

IntechOpen